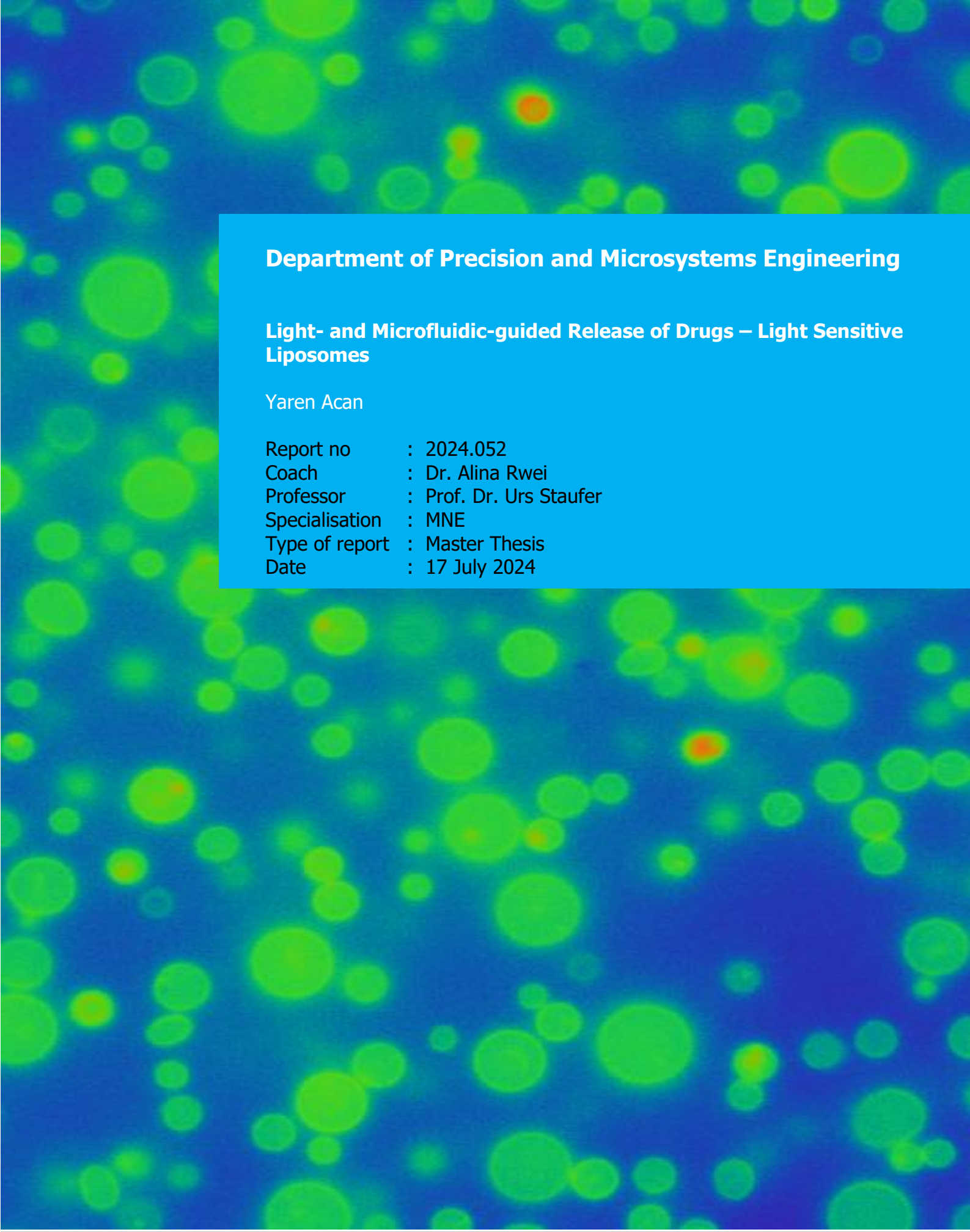

Department of Precision and Microsystems Engineering

Light- and Microfluidic-guided Release of Drugs – Light Sensitive Liposomes

Yaren Acan

Report no	:	2024.052
Coach	:	Dr. Alina Rwei
Professor	:	Prof. Dr. Urs Staufer
Specialisation	:	MNE
Type of report	:	Master Thesis
Date	:	17 July 2024

Light- and Microfluid-guided Release of Drugs

Light Sensitive Liposomes

by

Yaren Acan

Student Name	Student Number
Yaren Acan	5734649

Chair:	Urs Staufer
Supervisor:	Alina Y. Rwei
Daily Supervisor:	Ignasi Simon Grau
Project Duration:	09,2023 - 07,2024
Faculty:	Mechanical Engineering (ME) & Applied Sciences (AS)

TU Delft

Acknowledgement

I would like to extend my heartfelt gratitude to several individuals and groups who have been instrumental in the completion of this thesis.

First and foremost, I am deeply thankful to my supervisors, Dr. Alina Rwei and Prof. Dr. Urs Staufer, for their invaluable guidance, support, and unwavering belief in my abilities. Their expertise, patience, and insightful feedback have been crucial in shaping and refining this research.

I am also indebted to Dr. Ida Kokalari, Ignasi Simon Grau and Nikki Nafar, whose assistance in the lab and willingness to share their expertise greatly contributed to the success of this study. Their support was invaluable in overcoming challenges and achieving milestones throughout the research process.

To my family, whose unconditional love, encouragement, and understanding have sustained me throughout my academic journey, I express my profound gratitude. Your unwavering support has been my pillar of strength.

To my friends, who have cheered me on, listened patiently and provided much-needed breaks and laughter during intense periods of study, I am incredibly grateful.

Lastly, I would like to thank to Joel Häggström, for his constant love, support, and encouragement. His belief in me and his willingness to stand by my side through thick and thin have been a source of inspiration.

To all those mentioned above and to those who supported me in various ways but are not named here, I extend my sincerest thanks. This thesis would not have been possible without your contributions and encouragement.

Yaren Acan
Delft, July 2024

Abstract

Each year, stroke claims about 5.5 million lives and leaves around 116 million with lasting disabilities. Current stroke treatments focus on the acute phase, lacking drugs for neuron protection or damage repair due to the blood-brain barrier. This proof-of-concept project presents an implantable drug delivery system (DDS) using microfluidics and light-sensitive liposomes for post-stroke treatment in the affected regions of the brain. This research investigates the synthesis, characterization, and application of giant unilamellar vesicles (GUVs) for potential drug delivery applications. Vesicles synthesized by the gel-assisted swelling method. Dye encapsulation studies identified 5 µM as the optimal concentration, with higher concentrations negatively impacting vesicle formation. Stability assessments showed that PEGylation and cholesterol enrichment improved thermal stability and encapsulation efficiency, with lower temperatures generally enhancing stability. Coating GUVs with gold nanoparticles faced challenges with aggregation, indicating the need for optimized reagent concentrations and reduction processes. Dye release studies demonstrated stable encapsulation up to 39°C, suggesting potential for controlled release via surface plasmon resonance. Pipetting was found to better preserve vesicle integrity in microfluidic platforms compared to syringe introduction. Overall, this thesis provides comprehensive knowledge about the synthesis, lipid formulation optimization, and stability of GUVs, offering practical insights into their handling and application in microfluidic platforms, and laying the groundwork for future innovations in drug delivery systems.

Contents

List of Figures

List of Abbreviations

FDA	Food and Drug Administration
rt-PA	Recombinant tissue plasminogen activator
CNS	Central nervous system
BBB	Blood-brain barrier
9-AA	9-Aminoacridine
DDS	Drug delivery system
GUV	Giant unilamellar vesicle
ULV	Unilamellar vesicles
OLV	Oligolamellar vesicle
MLV	Multilamellar vesicle
MVV	Multivesicular vesicle
LUV	Large unilamellar vesicle
SUV	Small unilamellar vesicle
DPPC	1,2-dipalmitoyl-sn-glycero-3-phosphocholine
DOPC	1,2-dioleoyl-sn-glycero-3-phosphocholine
Chol	Cholesterol
DSPE-PEG2000	1,2-distearoyl-sn-glycero-3-phosphoethanolamine-N-[amino(polyethylene glycol)-2000] (ammonium salt)
k_B	Boltzmann constant
T	Temperature
OLA	Octanol-assisted liposome assembly
c-DICE	Continuous-droplet interface cross encapsulation
e-DICE	Emulsion-droplet interface cross encapsulation
PVA	Polyvinylalcohol
T_m	Phase transition temperature
EE	Encapsulation efficiency
d	Diameter
s_p	Pixel size
A	Area
OCT	Optical coherence tomography
PDT	Photodynamic therapy
LED	Light-emitting diode
ANSI	American National Standards Institute
UV	Ultraviolet
NIR	Near-infrared

Vis	Visible
ROS	Reactive oxygen species
SPR	Surface plasmon resonance
AuNP	Gold nanoparticle
$HAuCl_4 \cdot 3H_2O$	Tetrachloroauric(III) acid trihydrate
l-AA	l-Ascorbic acid
Au^{+3}	Gold ion
Au^{0}	Elemental gold
SRhoB	Sulforhodamine B
Tris-HCl	Tris(hydroxymethyl)amino-methane hydrochloride
KCl	Potassium chloride

1

Introduction

A stroke is when there's a sudden issue with blood flow in a specific part of the central nervous system, typically caused by a vascular problem [1]. It's split into two types: ischemic and hemorrhagic. Globally, strokes cause a lot of deaths and disabilities and come with significant costs for care after a stroke. While the number of stroke-related deaths and cases has dropped, the overall impact of strokes remains high, according to the 2016 Global Burden of Diseases Report [2]. Right now, the only FDA-approved treatment for ischemic stroke is a drug called recombinant tissue plasminogen activator (rt-PA or Alteplase). However, it has a limited window for effectiveness, meaning only 7% of eligible patients can benefit from it [1].

Researchers have been investigating the use of liposomes, small lipid-based vesicles, to enhance the treatment of brain diseases. Liposomes can transport both fat-soluble and water-soluble substances, including drugs, proteins, and genetic materials [3]. They are biocompatible, have a low likelihood of triggering an immune response, and can be designed to respond to specific stimuli such as light, ultrasound, or pH changes. The project aims to integrate these lipid vesicles into a microfluidic platform to improve the spatiotemporal control and efficacy of the drug within the affected brain area, bypassing the need to cross the blood-brain barrier (BBB).

1.1. Stroke

1.1.1. Pathophysiology of stroke

Stroke is a pathological condition arising from diminished blood flow to a specific brain, retina, or spinal cord region. It leads to a lack of oxygen and glucose supply to nearby cells and reduces it for distant cells. Following a stroke, reperfusion occurs when blood flow is restored, and the tissue receives oxygen again [1].

There are two main types of stroke: ischemic and hemorrhagic. Ischemic strokes result from a blockage in a vessel caused by clotting, platelet aggregation, or atherosclerosis, halting blood flow [1]. Hemorrhagic strokes happen when a vessel ruptures, causing blood to leak into the parenchyma [4].

Post an ischemic stroke, the affected area shows two distinct regions: the core and the penumbra. The core, closest to the disrupted blood flow, experiences the most cell death. In the ischemic penumbra, cells are damaged but potentially reparable if circulation is quickly restored [5]. Cells in the core, where blood flow drops significantly, die from necrosis, while the surrounding penumbra remains viable. This clinically crucial penumbra area holds more significance for recovery than the infarct volume itself (Fig. 1.1). As this region is potentially recoverable, various studies aim to shield it from stroke's damaging effects, underscoring the need for new medications in stroke treatment [5].

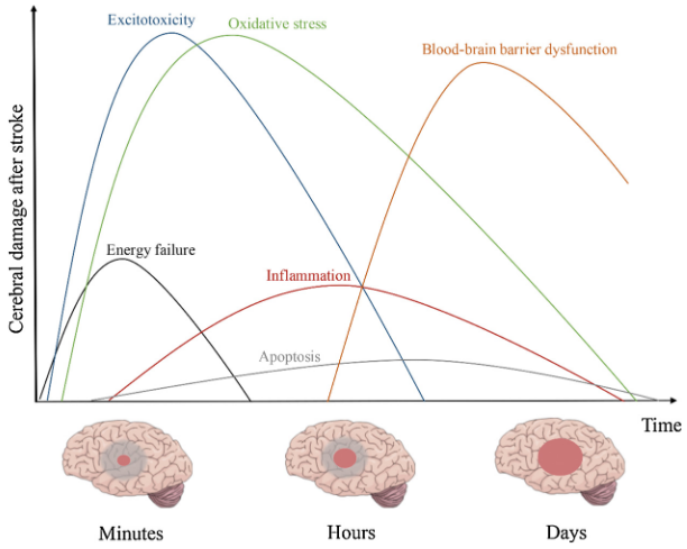

Figure 1.1: The illustration of the chronological progression of the primary pathophysiological processes causing cerebral damage post-stroke. It showcases the ischemic penumbra in gray and the infarcted core in red [6].

1.1.2. State-of-the-art of stroke treatment

As of now, there is only one FDA-approved medication, recombinant tissue plasminogen activator (rt-PA), for treating ischemic stroke. This drug dissolves blood clots in cerebral vessels, restoring blood flow and safeguarding ischemic brain tissue. However, its administration requires precise dosing and timing due to its potential risks [1]. The standard intravenous dose given within the initial 4–5 hours after an ischemic stroke is 0.9 mg/kg. Although this dosage increases the chances of minimal disability at 3–6 months without impacting mortality, it also elevates the risk of symptomatic intracerebral hemorrhage. Lowering the dose to 0.6 mg/kg reduces the incidence of hemorrhage but doesn't improve functional outcomes compared to the standard dose [7].

Apart from rt-PA, mechanical thrombectomy stands as another treatment option, surgically restoring blood flow in large cerebral arteries more effectively than thrombolysis alone. Despite showing advantages over rt-PA treatment individually, enhancing the technological aspects of this procedure and broadening its accessibility across hospitals remain crucial [8].

Unfortunately, no pharmacological treatments have significantly improved functional outcomes in hemorrhagic stroke patients. Surgical evacuation or minimally invasive drainage via catheter might benefit some patients with supratentorial hematomas, but these options are limited [9].

Given the inadequacies of current treatments, there's an urgent need for new stroke treatment strategies. While neuroprotective drugs have shown promise in animal models, they've struggled to demonstrate clinical effectiveness. To address this, scientists are exploring nanotechnology, particularly liposomes, to enhance the therapeutic potential of various substances for stroke treatment.

Liposomes, the first generation of drug nanocarriers, are vesicles made of a phospholipid bilayer enclosing an inner aqueous compartment, resembling cell membranes [3]. Their structure allows encapsulation of both hydrophilic and lipophilic compounds, offering versatility in drug delivery. This encapsulation shields drugs from degradation, immune responses, and clearance, prolonging their half-life. Moreover, as a central nervous system (CNS) nanocarrier, liposomes have been studied extensively due to their ability to aid in crossing the blood-brain barrier (BBB), a hurdle in drug delivery to the brain [10].

Numerous in vivo studies have investigated liposomal drug formulations to heighten therapeutic effects. Researchers have explored anti-inflammatory therapies to enhance motor activity in stroke patients using liposomal drug delivery. Wang et al. proposed the use of 9-Aminoacridine (9-AA), an FDA-approved

drug, encapsulated in liposomes to suppress neuroinflammation in the penumbra within two weeks post-stroke, achieving promising results in animal models [11]. Ishii et al. also utilized another FDA-approved drug, FK506, achieving comparable outcomes in rat models. Numerous other experiments have explored the administration of liposomal drugs in the penumbra region in animal models [12].

However, a significant challenge in this research lies in controlling the spatial and temporal release of drugs. While these proposed liposomal formulations outperform sole-drug administrations, some still exhibit adverse effects on the liver [11]. To address this issue, stimuli-responsive liposomes can be utilized. These liposomes are used for several different brain drug delivery systems with promising results such as enabling controlled drug release at specific locations and times [13]. Light-sensitive liposomes incorporate light-sensitive components that regulate drug release, aiming to overcome the limitations of traditional liposomes.

1.2. Proposed drug-delivery system of stroke

To tackle the challenges of drug delivery for stroke recovery, a drug delivery system (DDS) combining a microfluidic platform and liposomes is proposed. This proposed DDS aims to enhance drug efficacy and spatiotemporal control by bypassing the BBB with the microfluidic device and ensuring drug release only when the liposome is activated by an external stimulus, such as light. Typically, liposomes that are used for drug delivery are at the nanometer scale, but due to fabrication limitations of the microfluidic platform, micrometer-sized liposomes, known as giant unilamellar vesicles (GUVs), are necessary for the proposed DDS. These GUVs, commonly used in synthetic cell studies due to their size compatibility with eukaryotic cells, are suggested as drug delivery agents by many researchers for their potential in enhanced encapsulation efficiency and stability[14], [15]. Despite their potential, this area remains underexplored. This thesis aims to investigate the potential of GUVs as drug delivery agents by examining their encapsulation efficiency, stability at various temperatures over time, and their behavior within a microfluidic platform. Additionally, the study explores coating GUVs with light-sensitive nanoparticles (gold nanoparticles) to evaluate their use as external stimuli-responsive drug carriers. For more detailed information on the microfluidic platform design, fabrication, and testing, refer to the master thesis of Gijs van Veen, who collaborated on this project.

To answer these questions, dye-loaded GUVs were synthesized using the gel-assisted swelling method and tested for stability at 4°C, 25°C, and 37°C for up to two weeks. These vesicles were then incorporated into a microfluidic platform, where pressure-induced bursts were observed (see the thesis of Gijs van Veen). Efforts to grow gold nanoparticles on the GUV surface for light-triggered drug release did not achieve proper coating. However, thermal-induced cargo release was successfully demonstrated through bulk heating of the GUVs, laying the groundwork for future research.

This report covers the theory behind the proposed mechanism, synthesis methods, and subsequent studies on GUVs, including their incorporation into the microfluidic platform. It details the theoretical background of light-sensitive liposomes, their synthesis techniques, light as a cargo release mechanism, and the interaction between light and liposomes (See Section 2). The materials and methods used in the project are reported in Section 3, with results presented and discussed in Section 4. Section 5 concludes the project by highlighting key findings, and Section 6 offers recommendations for future studies.

2

Theoretical background

2.1. Liposomes

Liposomes, which are lipid vesicles created through self-assembly, can enclose both hydrophilic and hydrophobic substances. First identified by A.D. Bangham in the mid-1960s [16], these structures are among the earliest nanocarrier systems. Their sizes can vary from a few nanometers to several hundred micrometers. For this project, due to constraints in microfabrication techniques, the required liposome size to be studied and produced was in the micrometer range. These are known as giant unilamellar vesicles (GUVs). The initial section (Section 2.1) primarily covers the theoretical background of giant unilamellar vesicles, detailing their structure, composition, preparation methods, and characterization techniques. The subsequent section (Section 2.2) examines the interaction between light and liposomes and discusses the potential use of this system as a light-sensitive drug delivery mechanism.

2.1.1. Structure, composition and classification

Liposomes are vesicles characterized by one or more lipid bilayers. Each liposome is composed of either naturally occurring lipids or synthetic amphiphiles, featuring two hydrophobic tails and a hydrophilic head (2.1 A). These molecules self-assemble into double layers with the hydrophilic heads facing outward, interacting with the surrounding aqueous solution, and the hydrophobic tails facing inward, forming a hydrophobic core. These double-layer membranes are known as lipid bilayers. The exposure of the hydrophobic core to water induces a high free energy penalty, leading bilayers to close naturally, resulting in the spherical structures known as liposomes or lipid bilayer vesicles [17].

Liposomes can be classified by their size and lamellarity into unilamellar vesicles (ULVs), oligolamellar vesicles (OLVs), multilamellar vesicles (MLVs), and multivesicular vesicles (MVVs), as depicted in Figure 2.2. OLVs and MLVs have an onion-like configuration, with 2–5 and more than 5 concentric lipid bilayers, respectively. In terms of particle size, ULVs are subdivided into small unilamellar vesicles (SUVs, 30–100 nm), large unilamellar vesicles (LUVs, >100 nm), and giant unilamellar vesicles (GUVs, >1000 nm) [18]. When hydrated, lipid films self-assemble into MLVs, which can then be converted into unilamellar SUVs or LUVs using methods such as sonication or extrusion [19].

Smaller vesicles excel in targeted delivery, while larger vesicles can improve loading capacity and stability. However, larger vesicles may impede efficient tissue penetration and targeting. Conversely, multilayer vesicles have a high encapsulation capacity but may face challenges regarding stability and immune system recognition [20].

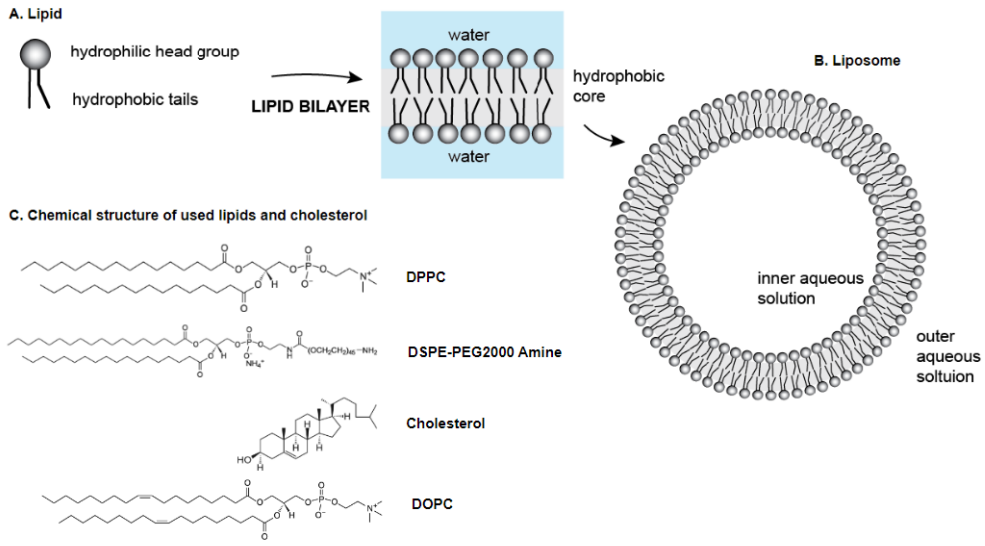

Figure 2.1: (A) Structure of lipid, (B) Structure of a liposome [17], (C) Structure of 1,2-dipalmitoyl-sn-glycero-3-phosphocholine (DPPC)[21], 1,2-distearoyl-sn-glycero-3-phosphoethanolamine-N-[amino(polyethylene glycol)-2000] (ammonium salt) (DSPE-PEG2000) [22], and cholesterol [23], 1,2-dioleoyl-sn-glycero-3-phosphocholine (DOPC) [24].

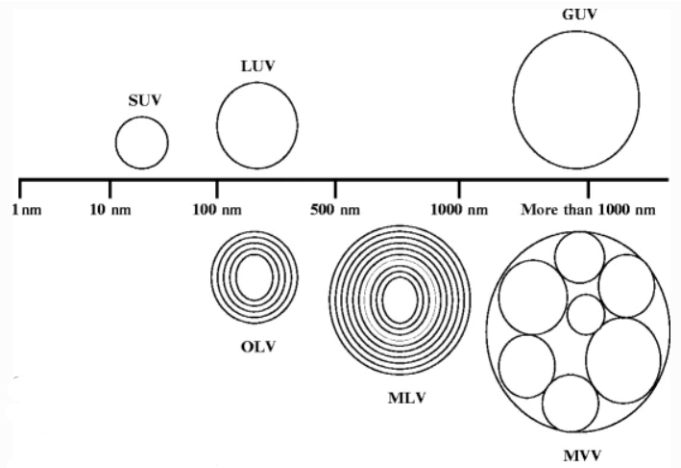

Figure 2.2: Size and lamellarity-based classification of liposomes [18]

Liposomes have distinctive physical properties, making them a significant research focus for applications ranging from drug delivery to artificial cell studies. Before delving into liposome synthesis, it is essential to discuss some key characteristics.

Permeability: Due to their hydrophobic core, lipid bilayers allow hydrophobic molecules and small uncharged polar molecules like water to pass through, but they are impermeable to protons, ions, and large uncharged polar molecules such as proteins and sugars.

Fluidity: The lipids in bilayers are held together by non-covalent interactions, which are relatively weak. These interactions permit the lateral movement of lipids within the membrane, resulting in lateral diffusion and contributing to the bilayer's fluid nature.

Elasticity: Lipid membranes are mainly deformed by stretch and curvature deformations [25]. They have a low bending modulus of 10-30 k_BT, allowing them to easily bend out-of-plane due to their small bilayer thickness (6 nm) [17]. Membranes can spontaneously bend due to thermal fluctuations in the surrounding solvent. Unlike bending, bilayers are highly resistant to stretching deformations. The

stretch moduli of bare lipid membranes typically range between 100-300 mN/m [26]. Due to their fluid nature, local stretching of the bilayer quickly equilibrates across the entire membrane. While bending deformations dominate at low membrane tensions, stretching occurs at high tensions [27]. When membrane tension exceeds the lysis tension (4-10 mN/m), or 4-10% strain, depending on bilayer composition [28], [29], the membrane ruptures.

Diversity: Lipids exhibit great diversity in structure and properties. Although they all have a hydrophilic head and hydrophobic tails, they vary in head group size and charge, hydrocarbon tail length, and tail saturation. These lipid properties influence interactions within the bilayer, affecting elasticity, fluidity, and interactions with the external environment [30], [31]. Cholesterol is also an important component of many liposome formulations, integrating into the bilayer and affecting lipid packing, which impacts liposome fluidity, permeability, and elasticity [20].

2.1.2. Preparation methods

The primary methods for preparing liposomes vary, largely based on their size. Common techniques for producing SUVs, LUVs, OLVs, and MLVs include thin-film hydration, reverse-phase evaporation, ethanol injection, freeze-thaw, double emulsion, and extrusion [32]. Among these, thin-film hydration and reverse-phase evaporation are the most frequently cited methods in the literature.

For the synthesis of GUVs, various techniques have been developed, which fall into two main categories: swelling-based and emulsion-based methods. Swelling-based methods involve creating a thin film layer and then swelling it using techniques such as electroformation, gel-assisted swelling, and spontaneous swelling. The emulsion-based method constructs vesicles in steps: first, forming water droplets in a nonpolar solvent surrounded by a single lipid layer, then 'enwrapping' these droplets with a second lipid layer to create the vesicular structure. This can be achieved through methods like inverse emulsion, Octanol-assisted Liposome Assembly (OLA) microfluidics, continuous droplet interface crossing encapsulation (cDICE), and emulsion droplet interface crossing encapsulation (eDICE). An illustration of each technique is provided in Figure 2.3. To select the most appropriate synthesis method, a table comparing the pros and cons of each method is prepared and shown in Table 2.1. Based on parameters such as training time, yield of GUVs, size distribution, and the available lab equipment, the Gel-Assisted Swelling method was chosen to synthesize GUVs for this project.

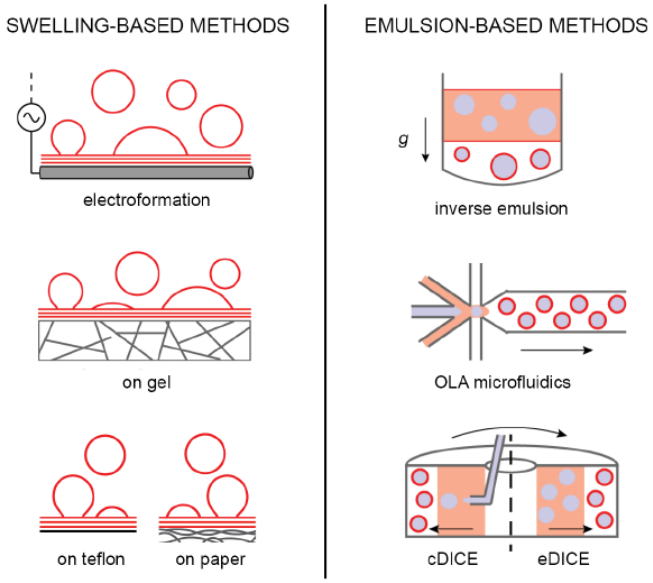

Figure 2.3: Schematic overview of the GUV synthesis techniques. Left: Swelling-based methods. Right: Emulsion-based methods [17]

Table 2.1: Comparison of different GUV synthesis methods based on their advantages and limitations

Method	Sub-Method	Advantages	Limitations
Swelling-Based	Electroformation	High yield of GUVs	Requires optimization for each condition (based on lipids and buffers)
		Lots of literature	Lengthy training time (2 months)
			Not compatible with charged lipids/buffers
			Polydisperse GUVs
	Gel-assisted Swelling	Robust and easy to use	Gel thickness is crucial
		High yield of GUVs	Potential contamination with gel polymers
		Shorter training time (2 weeks)	Polydisperse GUVs
		Vesicle size up to 50 µm	
		Compatible with charged lipids and buffers	
	Spontaneous Swelling	Simple implementation	Long swelling time
		Clean membrane	Polydisperse GUVs
Emulsion-Based	Inverse Emulsion	Quick and easy	Variable encapsulation efficiency
		Control over vesicle content	Reduced yield with high ionic strength
		Shorter training time (<1 months)	Polydisperse GUVs
	OLA Microfluidics	Control over vesicle size and content	Lengthy training time (3-8 months)
		In situ observation	Complex pretreatment
			Prone to channel clogging/leakage
	eDICE - cDICE	Easier to execute than OLA microfluidics	Limited shape control
		Suitable with physiological conditions of charged lipids and ionic solutions	Variable encapsulation efficiency

Preparation of giant unilamellar vesicles: Gel-assisted swelling

The gel-assisted swelling method employs a polymer-based gel as a substrate on which a thin lipid film is spread. The swelling process is expedited by a flow of buffer that enters beneath the bilayers on a porous polymer layer (Fig. 2.4) [33]. This technique is advantageous compared to other swelling-based methods due to its short synthesis time, short training time, no requirement for further optimization, and high yield of GUVs.

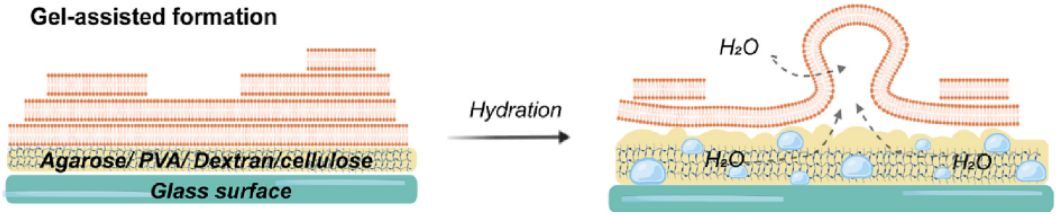

Figure 2.4: Illustration of the gel-assisted swelling synthesis of GUVs [34]

In detail, the synthesis begins by spreading a polymer-based gel (e.g., Poly-vinyl alcohol (PVA)) on a glass slide. After baking the gel according to the polymer used, a thin lipid film is spread on the gel. The excess organic solvent in the lipid film is evaporated in a desiccator for half an hour. After solvent evaporation, a swelling buffer, adjusted according to the lipid used, is carefully added on top of the lipid film without disturbing it. The vesicles start to grow immediately. The produced vesicles can be harvested by either tapping the bottom of the swelling chamber or flushing the swelling solution over the tilted gel. Although GUVs can be harvested after several minutes, extending the swelling time up to an hour can reduce the presence of secondary membrane structures on vesicles [17].

Gel-assisted swelling is a robust and highly compatible technique with various lipid formulations. It is an optimized method for GUV synthesis, requiring minimal training and offering quick production with a high yield. Additionally, cargo encapsulation can be achieved by adding the desired cargo into the swelling buffer [17]. However, the success of the synthesis heavily depends on several parameters, which are listed as follows.

- GUV creation requires a gel attachment to the supporting glass coverslip. Cracking of the gel upon addition of the swelling solution could be seen if the gel is not sticking to the glass well or if it is very thick. GUV formation fails in the event of gel cracking [17]. The glass surface needs to be treated by plasma treatment before the gel is distributed to prevent cracking. For the gel solution to be more viscous and capable of spreading as a thinner gel layer, it should always be brought to room temperature. High swelling temperatures could be another cause of gel cracking [35].
- The swelling buffer and temperature should be adjusted in accordance with the composition of the membrane. For instance, the swelling buffer should be ionic when working with charged membranes since non-ionic buffers cause the lipid film to separate from the gel [17]. Similarly, the swelling temperature needs to be modified based on the phase transition temperature (T_m) of the lipids utilized. To prevent the lipid film from detaching, swelling should be carried out at 50°C for DPPC lipids (T_m of 41 °C).
- Buffering the swelling solution will reduce the adhesion between neighboring GUVs [36]. The addition of buffer likely changed the pH of the solution relative to the lipids' isoelectric point, which changes the net charge of the lipids.
- One critical factor influencing the success of vesicle formation is the presence of sugar during the formation process. Sucrose enhances GUV formation by increasing the hydrodynamic force on the lipids through a rise in inter-facial viscosity between the solution and the lipid membrane [37]. Van Burren found that yields were exceptionally high at 500 mOsm sucrose in the swelling solution, whereas hardly any vesicles formed at 20 mOsm sucrose [17]. Additionally, higher sugar concentrations result in fewer secondary membrane structures [36]. Since sugar is known to modify membrane properties such as bending rigidity, its interaction with the membrane may facilitate the creation of GUVs [38].

2.1.3. Characterization methods

By far the most common characterization technique for GUVs is optical microscopy. GUVs can be imaged in a bright field or a fluorescence microscope with the inclusion of dyes, either membrane-bound or encapsulated. Most studies with GUVs involve simple wide-field or confocal microscopy, as well as super-resolution microscopy. However, to enhance the understanding of the characteristics of the produced GUVs, quantitative image analysis should be performed on the obtained microscopy images. This image analysis could be done manually or custom-made scripts are used to process specific data sets and generate a pre-defined set of output parameters [36].

Determining phospholipid content is not typically a characterization technique for GUVs since they are typically used for synthetic cell studies. However, in the context of drug delivery systems, where lipid formulations are designed to meet specific requirements and ensure batch consistency for the same therapeutic effect, phospholipid content determination becomes a crucial aspect of liposome characterization.
Within the scope of this project, fluorescence microscopy was adapted due to its accessibility and ease of use for determining the size and encapsulation efficiency of GUVs. This technique allows for detailed visualization and measurement of the vesicles, providing crucial data on their structural properties and the efficiency with which they encapsulate materials. Additionally, phospholipid content was determined using the Stewart assay. This method is essential for quantifying the amount of phospholipid in the liposomes, ensuring the consistency and accuracy of the lipid formulation used in the drug delivery system. By combining these techniques, the project aims to comprehensively characterize GUVs for their potential application in targeted drug delivery.

Size and encapsulation efficiency determination: Fluorescence microscopy & Image Processing

Fluorescence Microscopy A fluorescence microscope is an optical microscope that uses fluorescence and phosphorescence instead of, or in addition to, reflection and absorption to study the properties of inorganic or organic substances.

Fluorescence is the emission of light by a substance that has absorbed light or other electromagnetic radiation while phosphorescence is a specific type of photoluminescence related to fluorescence [39].

The main step in observation of the sample includes labeling the sample with fluorescent dye. Then, the light source that emits white light falls onto the excitation filter. This filter selects the light of a specific wavelength that can excite the fluorescent molecules tagged in the specimen and this excited light incidents onto the dichroic mirror. The light after reflection from the dichroic mirror passes onto the specimen after emerging from the objective lens. This smaller wavelength light falls into the specimen tagged with a fluorescent dye that results in the emission of high-wavelength light which passes again through the condenser lens and dichroic mirror. This allows high-wavelength light to pass towards the emission filter which only permits longer-wavelength light to pass into the eyepiece and detector while rejecting the shorter-wavelength light completely. The detector detects the higher-wavelength light and permits it to fall back onto the specimen thereby, forming fluorescent green specimens against a dark background [39].

Typical components of a fluorescence microscope are a light source (e.g., xenon arc lamp, mercury-vapor lamp, high-power LEDs, lasers), the excitation filter, the dichroic mirror, and the emission filter. The filters and dichroic mirror should be chosen to match the spectral excitation and emission characteristics of the fluorophore used to label the specimen. The distribution of a single fluorophore (color) is imaged at a time. Multi-color images of several types of fluorophores must be composed by combining several single-color images [40].

Most fluorescence microscopes in use are epifluorescence microscopes, where excitation of the fluorophore and detection of the fluorescence are done through the same light path. Schematic of an inverted fluorescence microscope can be seen in Figure 2.5.

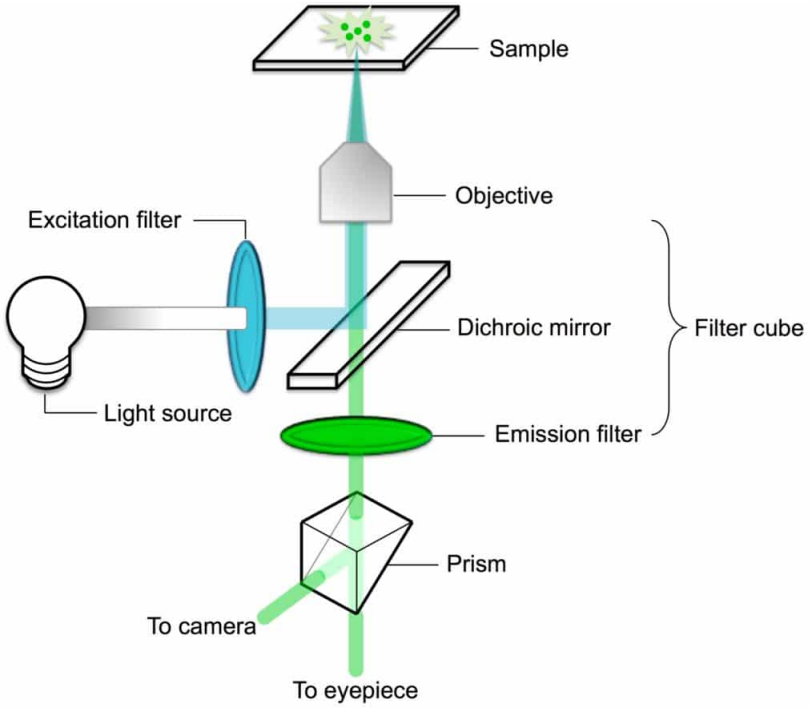

Figure 2.5: Schematic of an inverted fluorescent microscope, showing the components and the light path [41].

Even though, fluorescence microscope is commonly used for various applications such as cell biology and material sciences due to its ease of use, adaptability, sensitivity, and reliability; it compasses several limitations. One of the main limitations is the photobleaching which occurs due to the accumulated chemical damage caused by the light on fluorescent molecules. Photobleaching causes fluorophores to lose their ability to fluoresce and severely limits the time the sample can be observed by fluorescence microscopy. To reduce photobleaching several techniques can be applied such as minimizing illumination and using photoprotective chemicals [39]. Another limitation is the probes and dyes added to the membrane of liposomes can alter the characteristics of the bilayer if it exceeds a certain mole percent [42].

In addition to labeling the sample with a fluorescent label, another important part of imaging GUVs with a fluorescent microscope is the preparation of the sample and the imaging chamber. Imaging of GUVs requires a well-imaging chamber. To minimize the surface adhesion between the chamber and the GUVs, the surface of the imaging chamber should be passivated. Also, in the case of using an inverted microscope, GUVs should immobilized on the bottom of the imaging chamber. The easiest way to immobilize GUVs is to create a density difference by using a similar osmolarity but less dense buffer as an observation buffer [42]. For example, a GUV that has been swelled with a 200 mOsm sucrose buffer should be observed with a glucose buffer with the same osmolarity.

Image Processing Due to their size in the range of 5-100 µm, optical microscopy is a widely used technique for the characterization of GUVs. Despite the experimental ease of imaging GUVs, their quantitative imaging analysis has received relatively little attention from researchers [36]. The most commonly adopted methods are imaging GUVs by brightfield, phase-contrast or fluorescent microscopy, and image processing by ImageJ [36].

ImageJ is a public domain software for processing and analyzing scientific images developed at the National Institutes of Health and Laboratory for Optical and Computational Instrumentation (LOCI, University of Wisconsin) [43]. ImageJ can calculate the area and pixel value statistics of user-defined selections within an image [44].

In the case of GUV characterization, the liposome diameter and fluorescent intensity within the GUVs

can be calculated by using the area and pixel value statistics obtained by ImageJ. In the case of size determination, by utilizing the circular phase of GUVs, area information can be used to obtain diameter by using the area of a circle formulation 2.1.

$$d = 2s_p\sqrt{\frac{A}{\pi}} \tag{2.1}$$

Where d is the diameter of the GUV, s_p is the pixel size of the microscopy image and A is the total area of a GUV in terms of pixels value obtained by ImageJ.

Fluorescent intensity can be used for encapsulation efficiency calculations, which is another important aspect of liposome characterization. Encapsulation efficiency is a measure to determine the success of entrapment of the cargo within liposomes and it can be calculated as Equation 2.2.

$$\text{EE} = \frac{\text{mass of cargo encapsulated}}{\text{mass of total cargo loaded}}\text{x100\%} \tag{2.2}$$

Firstly, a calibration curve should be created by using varying amounts of dye concentrations to determine the absolute amount of dye encapsulated. The fluorescent intensity of these samples should be determined. Then by using the obtained calibration curve, the amount of dye encapsulated within a liposome can be obtained by measuring the individual encapsulated dye fluorescent intensity within the GUVs.

Phospholipid content: Stewart assay

Since lipid formulation has been developed to satisfy a specific requirement in the drug delivery system and to standardize each batch to obtain the same therapeutic effect, phospholipid content determination is an essential component of liposome characterization. It is also a crucial component of medication stability, release rate, and incorporation. Despite the development of other quantification techniques, this study used Stewart Assay, which is the most straightforward technique. The Stewart Assay is a colorimetric technique that relies on the phospholipid headgroups and ammonium ferrothiocyanate forming a red-colored complex that can be measured spectrophotometrically after being extracted into chloroform [45]. To be more precise, the liposome sample is dissolved in chloroform and combined with the reagent ammonium ferrothiocyanate. Despite its insolubility in chloroform, the reagent combines with phospholipids to generate a complex that is easily soluble in the solvent (Fig.2.6). The optical density of the chloroform phase is then measured at 470 nm after the two phases are separated. By using the Beer-Lambert law 2.3, the obtained absorbance can be further converted into total lipid concentration.

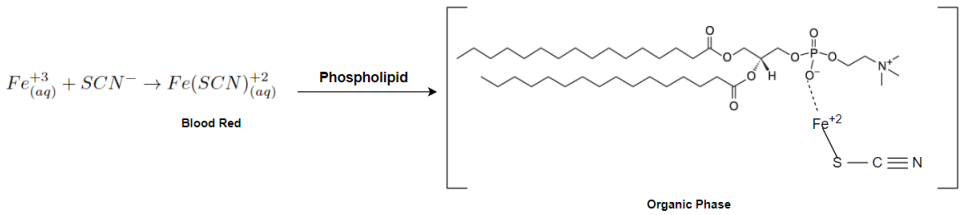

Figure 2.6: Reaction mechanism of Stewart assay

$$A = abc \tag{2.3}$$

Where A is the absorbance, a is the absorptivity of the absorbing species, b is the length of the beam in the absorbing medium and c is the concentration of the absorbing species. Since a and b are constants, the concentration and absorbance are proportionate. The analyte's concentration can be determined using the fitting equation in conjunction with the calibration curve produced by matching standards.

2.2. Light as a triggering modality

Due to the limitations observed in conventional liposomes for drug delivery purposes, researchers have explored novel approaches to enhance the efficacy and precision of drug delivery systems [13]. They have devised strategies to create liposomes responsive to internal (like acidic pH, high-temperature) or external stimuli (such as ultrasound, light, and magnetic fields). Internal stimuli are challenging to control and result in relatively slower drug release, on the other hand, external stimuli offer greater tunability for spatially and temporally sustained drug release [46]. However, external stimuli also have their drawbacks for example, ultrasound requires a responsive medium and can cause tissue damage with high-intensity applications; magnetic fields are costly, complex, and may involve potential toxicity due to metal usage [46]. Considering the system requirements set in the Introduction (Chapter 1), light emerges as the most suitable stimulus. One primary reason for this preference is its superior focus compared to other external stimuli methods, coupled with a wide range of operation wavelengths. Additionally, various light parameters like wavelength, exposure duration, light intensity, and beam diameter can be precisely adjusted to control drug release amount and timing [13].

Light, a defined segment of electromagnetic radiation, holds significant importance in biomedical disciplines, particularly for non-intrusive, accurate methods like diagnostics, and therapeutic applications, such as optical coherence tomography (OCT), photodynamic therapy (PDT) and photocoagulation [47]. In various studies, researchers utilize light to initiate drug release from diverse nanocarriers like liposomes, micelles, and metal nanoparticles [13] due to its exceptional spatiotemporal controllability.

Numerous light sources have been employed for therapeutic purposes including lasers, light-emitting diodes (LEDs), and X-rays. Choosing the appropriate light source relies on various factors. These factors include precision, power requirement, wavelength range, safety, cost, complexity, and flexibility. Lasers stand out for their remarkable precision attributed to their tightly focused and coherent beams. Conversely, LEDs offer a safer alternative, operating at lower power and voltages. They also present cost-effectiveness and simplicity when compared to laser systems.

The American National Standards Institute (ANSI) provides guidelines regarding the highest acceptable exposure levels to lasers and LEDs, primarily concerning ocular irradiation [48]. These standards are crucial considerations when choosing the suitable light source, as light can induce phototoxicity in biological tissues based on factors like intensity, wavelength, duration of exposure, laser pulse duration, and laser pulse intervals [48].

Both LED and laser devices can emit light across a wide range of wavelengths, spanning from ultraviolet (UV) to visible light and extending into the near-infrared (NIR) spectrum [48]. These varying wavelengths serve as triggering sources for controlled drug release from light-responsive liposomes encapsulating medications. The choice of specific light wavelengths relies on the light-sensitive molecule or moiety and the liposome composition, details of which will be further explained in the subsequent section (Section 2.2.1).

UV light (below 400 nm) and visible light (400-650 nm) are commonly used for medical purposes, as a single UV/Visible photon carries enough energy to induce photochemical reactions, extensively employed in light-sensitive liposomes [13]. Despite the advantages of UV/Vis-light such as higher energy and easier naked-eye observation, their limited tissue penetration depth poses a challenge. This range (200-650 nm) gets absorbed by various endogenous fluorophores like epidermis pigments, hemoglobin, and chlorophyll. For instance, energy around 400-600 nm gets absorbed significantly by skin chromophores like melanin and hemoglobin, impacting tissue penetration capacity of light within this range [13].

In contrast, NIR light demonstrates relatively lower absorption by hemoglobin and water, allowing deeper tissue penetration (up to 10 cm) without harming healthy tissue, making it advantageous in biomedical applications. However, wavelengths beyond 900 nm experience strong water molecule absorption. Therefore, the optimal therapeutic wavelength for in vivo settings typically falls between 650-900 nm, known as the first NIR window or optical window, offering millimeter-scale tissue penetration depth [49].

2.2.1. Mechanism of light-triggered drug release

Depending on whether the irradiation induces a chemical reaction within the lipid bilayer or initiates physical changes, the mechanism underlying the light-responsive liposomes can be categorized as either photochemical or photophysical activation, respectively. In both approaches, liposomes are engineered to destabilize the lipid bilayer and facilitate the release of contents trapped within the lipid vesicle upon irradiation [47].

There are several mechanisms that enable photochemical activation, including photoisomerization [50] [51], photocrosslinking [52], photocleavage [53] [54] [55], and light-induced oxidation [56] [57] [58]. Whereas, various methods of photophysical release have been devised utilizing light-absorbing components like molecular dyes [59] [60], plasmon-resonant nanoparticles [61] [62] [63], and inorganic nanomaterials [64] [65]. The table (Table 2.2) is given as a summary of the mentioned light-triggered drug release mechanisms based on their required wavelength for activation, the light-sensitive molecule within liposome, and a brief description of the mechanism.

Among these options, a selection could be made by considering their biocompatibility, release rate, activation wavelength, and applicability to the project. As shown in Table (Table 2.2), the cargo release is relatively less for photochemically activated liposomes. As well as the activation wavelength is in the UV range for azobenzene and o-nitrobenzyl which is highly dangerous considering the application area of the project is the brain. For the light-induced release, the liposome permeabilization is induced by reactive oxygen species (ROS) which is highly dangerous for live tissues [66]. On the other hand, molecular absorbers and inorganic nanoparticles hold limitations due to their biocompatibility [64], [50]. By considering these facts, plasmonic nanoparticles seem the most suitable liposome permeabilization technique. A more detailed explanation of the physics behind liposome permeabilization through plasmonic nanoparticle incorporation is given in the following section (Section 2.2.2).

2.2.2. Gold nanoparticle coated liposomes

Plasmonic nanoparticles exhibit unique optical properties due to their ability to interact strongly with light at specific wavelengths [68]. When exposed to light, these nanoparticles resonate with the incident electromagnetic field, leading to collective oscillations of their free electrons called surface plasmon resonance (SPR) [69]. This resonance results in enhanced light absorption and scattering, as well as localized electromagnetic field amplification in the vicinity of the nanoparticles. In the context of light-sensitive liposomes, plasmonic nanoparticles can serve as triggers for controlled drug release. By incorporating these nanoparticles into the liposomal membrane or encapsulating them within the liposome interior or coating liposomes with metallic nanoparticles, the nanoparticles can absorb specific wavelengths of light, converting the light energy into localized heat due to their plasmonic resonance (Fig. 2.7) [50]. This localized heat can induce changes in the liposomal membrane, leading to a controlled release of encapsulated drugs or therapeutic agents, thereby enabling precise spatiotemporal control over drug delivery in response to light [50].

Table 2.2: Summary of light-sensitive lipid permeabilization techniques [51], [52], [54], [57], [60], [62], [67].

Lipid Permeabilization Mechanism	Sub-Mechanism	Light-Sensitive Molecule(s)	Wavelength	Mechanism Explanation	Reference
Photochemical Activation	Photoisomerization	Azobenzene	UV/Vis	Azobenzene changes configuration depending on the wavelength. UV-light causes trans to cis configuration change and Vis range light reverse it. As a result constant opening and locking of the lipid membrane is possible	[51]
	Photocrosslinking	Photopolymerizable phospholipid (e.g. DC8,9PC)	UV/Vis	Polymerization of unsaturated bonds within the hydrophobic tail of the membrane upon illumination	[52]
	Photocleavage	o-nitrobenzyl	UV/Vis	Hydrolysis of o-nitrobenzyl upon irradiation causes separation of hydrophilic and hydrophobic segments of phospholipid	[54]
	Light-induced oxidation	Photosensitizers (Ce6, AlPcS2, 5,10-DiOH, PheoA)	UV/Vis	Oxidation of lipids within bilayer through reactive oxygen species (ROS) produced by photosensitizers upon irradiation	[57]
Photophysical Activation	Molecular absorbers	Lipophilic dyes (e.g. DiD)	Vis/NIR	Temperature increase above Tm of phospholipid due to photothermal conversion caused by molecular absorbers	[60]
	Plasmonic nanoparticles	Gold nanoparticles, silver nanoparticles	NIR	Temperature increase above Tm of phospholipid due to surface plasmon resonance phenomenon of noble metal nanoparticles	[62]
	Inorganic nanoparticles	Upconverting nanoparticles (e.g. Graphene oxide (GO), black phosphorous (BP))	NIR	Temperature increase above Tm of phospholipid due to electron state delocalization of upconverting nanoparticles	[67]

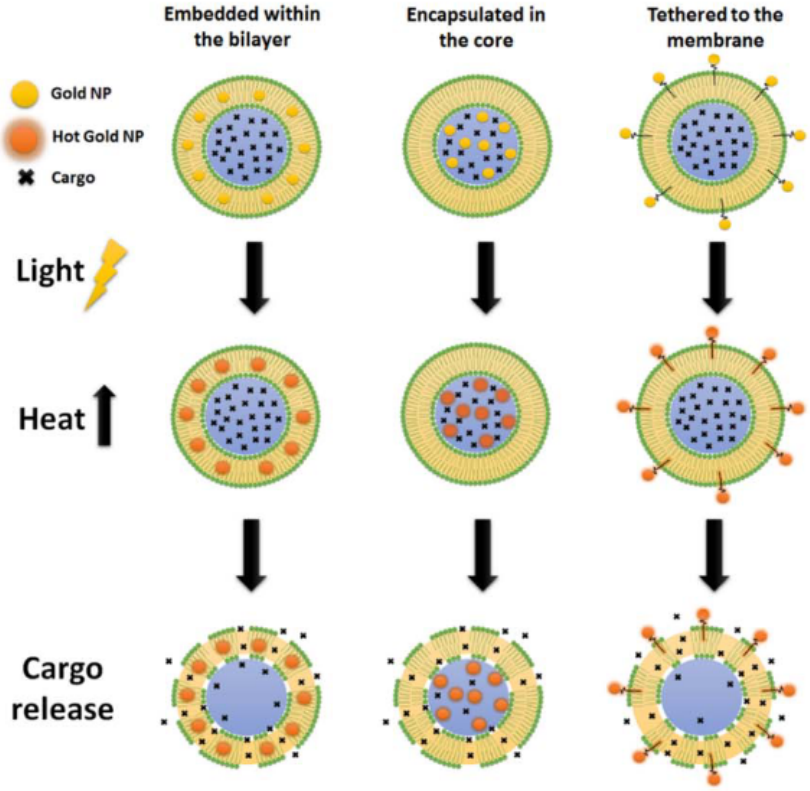

Figure 2.7: Liposomal photothermal release employing gold nanoparticles (NPs) can induce membrane disturbance through gold NPs positioned in various locations, including being embedded within the bilayer, enclosed in the core, or tethered to the membrane [50]

Surface Plasmon Resonance (SPR)

When light interacts with a metallic nanoparticle like gold, the unbound electrons within it start oscillating in response to the alternating electromagnetic field of the incoming light [68]. This synchronized electron movement on the metal surface results in a subtle division of overall charges, creating a dipole aligned with the light's electric field direction, depicted in Figure 2.8. At a distinct frequency or wavelength, known as the surface plasmon resonance (SPR), the extent of this oscillation peaks, leading to a heightened absorption of incoming light, typically quantified using a UV-Vis spectrometer [69].

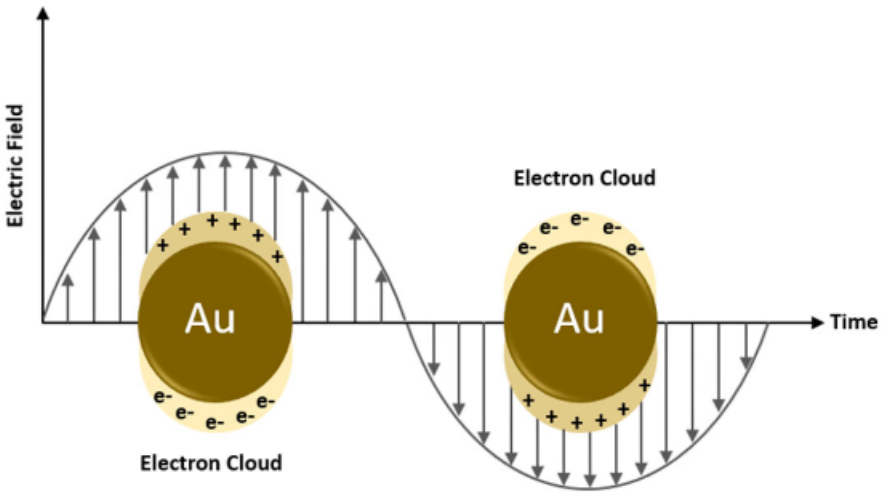

Figure 2.8: Schematic representation of surface plasmon effect (SPR) on gold nanoparticles [70]

When electromagnetic waves interact with such a nanoparticle, a portion of their energy dissipates through either light absorption or scattering processes. Absorption occurs when a photon's energy is lost through an inelastic process, where absorbed energy can be subsequently released as luminescence or heat. Metal nanoparticles tend to emit light poorly, thus absorbed photon energy is largely transformed into heat [61]. Conversely, light scattering arises when photon energy prompts electron oscillations, resulting in the emission of scattered light, either at the same frequency as the incident light or at a shifted frequency.

The degree of light absorption or scattering by the particle relies on absorption (C_{abs}) and scattering (C_{sca}) cross-sections [71]. To explain the optical attributes of spherical particles, the Mie theory was derived, resolving Maxwell's equations through a multipole expansion of electromagnetic fields [72]. When the particle size is significantly smaller than the incident light's wavelength (d « λ), a quasi-static approximation proves effective in describing optical properties [73]. This approximation assumes uniformity of electric charge across the entire particle [72]. Subsequently, Mie theory provides C_{abs} and C_{sca} as described in Equation 2.4 and Equation 2.5, respectively.

$$C_{abs} = kIm[\alpha] = 4\pi ka^3 Im[\frac{\epsilon(\omega) - \epsilon_m(\omega)}{\epsilon(\omega) + 2\epsilon_m(\omega)}] \tag{2.4}$$

$$C_{sca} = \frac{k^4}{6\pi}|\alpha|^2 = \frac{8\pi}{3}k^4\alpha^6|\frac{\epsilon(\omega) - \epsilon_m(\omega)}{\epsilon(\omega) + 2\epsilon_m(\omega)}|^2 \tag{2.5}$$

In these equations, where $k = \frac{2\pi}{\lambda}$ represents the wave number, λ signifies the wavelength, α denotes the polarizability, a indicates the particle radius, $\epsilon(\omega)$ signifies the frequency-dependent dielectric function of the material, and $\epsilon_m(\omega)$ denotes the frequency-dependent dielectric function of the medium. Examining these expressions reveals that absorption scales in proportion to a^3, whereas scattering scales proportion to a^6. This indicates that in smaller particles, absorption tends to dominate over scattering. However, as the particle size increases, scattering assumes greater importance. Consequently, smaller particles are preferred for photothermal applications, while larger particles prove more advantageous in imaging applications [68].

The combined values of scattering and absorbance cross-sections are termed as the extinction cross-section [72], denoted as C_{ext}, representing the complete attenuation of incoming radiation (Eq.2.6).

$$C_{ext} = C_{abs} + C_{sca} = 9\frac{\omega}{c}\epsilon_m^{3/2}V\frac{\epsilon_2}{[\epsilon_1 + 2\epsilon_m]^2 + \epsilon_2^2} \tag{2.6}$$

In this equation, ω denotes the frequency of the light, c represents the speed of light, V stands for the particle volume, and ϵ_1 and ϵ_2 correspond to the real and imaginary components of the dielectric function, respectively. Notably, the maximum extinction occurs when the Fröhlich condition $\epsilon_1 = -2\epsilon_m$ is satisfied. This highlights the reliance of SPR not solely on the particle's characteristics but also on the surrounding medium. Moreover, the attributes of the surrounding medium influence the positioning of the SPR peak. This occurrence finds an explanation through the Drude model [74], which shows interactions between free electrons and immobile positive ions in the metal. The real portion of the dielectric function derived from the Drude model can be expressed as:

$$\epsilon_1 = 1 - \frac{\omega_p^2}{\omega^2 + \gamma^2} \tag{2.7}$$

In this equation, ω_p represents the plasma frequency, while γ denotes the damping constant. By implementing the Fröhlich condition, converting the frequency to wavelength, and employing $\epsilon_m = n_m^2$, the resulting expression is as follows:

$$\lambda_{max} = \lambda_p\sqrt{2n_m^2 + 1} \tag{2.8}$$

In this equation, λ_{max} represents the wavelength at the SPR peak, λ_p stands for the plasma wavelength of the bulk metal, and n_m signifies the refractive index. Equation 2.8 illustrates that altering the refractive index causes a corresponding shift in the wavelength of the SPR peak. For instance, transitioning from water to silica as the medium would lead to a shift toward longer wavelengths.

Manipulating the size and shape of nanoparticles also allows for tuning the position of the SPR peak. As the size increases, particles are less uniformly polarized by incident light, leading to a redshift and broadening of the SPR peak [68]. This broadening becomes apparent in particles larger than 100 nm, where the retardation effects significantly influence it. Conversely, particles smaller than 10 nm display enhanced electron-surface interactions, resulting in phase changes and damping of the SPR peak [68]. Therefore, the optimal size range for gold nanoparticles falls between 10-100 nm. Figure 2.9 illustrates how size impacts both the position and broadening of the SPR peak [72].

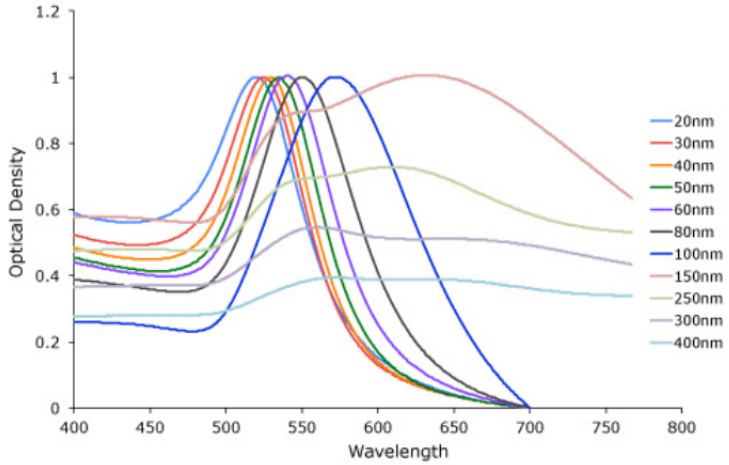

Figure 2.9: Size dependent surface plasmon effect (SPR) of gold nanoparticles [75]

Numerous nanoparticle shapes have been reported, such as rods, wires, triangles, shells, and cages. By changing the geometry, the position and the number of the SPR peak can be adjusted. For example, gold nanorods show two SPR peaks as compared to gold nanospheres that only exhibit one (Fig. 2.10). The first peak comes from excitation along the minor axis, while the second peak is caused by the excitation along the major axis [69].

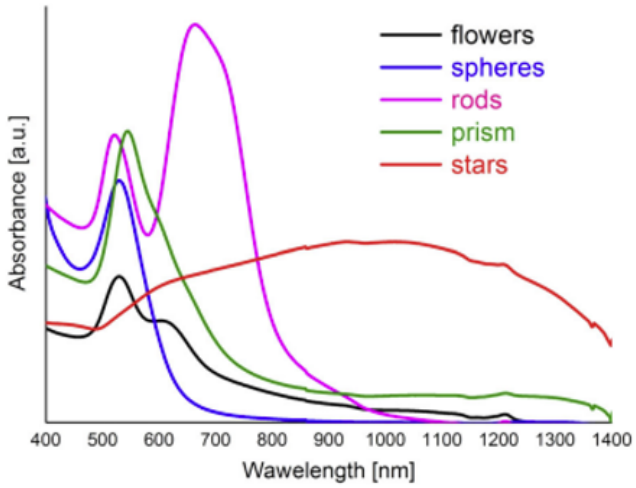

Figure 2.10: Effect of shape on the absorbance band of gold nanoparticles [76]

Gold nanoparticle (AuNP) - liposome nanocomposites

From a materials chemistry perspective, nanocomposites mix multiple materials to harness their combined advantages or to overcome limitations associated with individual components. It's essential to note that the term "nanocomposite" implies the presence of at least one component at the nanoscale [77].

Gold nanoparticles (AuNPs) have gained significant attention owing to their exceptional optical properties at the nanoscale, traced back to Michael Faraday's early colloidal gold synthesis, which marked the advent of gold nanoparticle research [78]. Over the years, a wealth of knowledge has been accumulated regarding the synthesis of gold nanostructures and a deeper understanding of their optical and photothermal traits [78].

The appeal of AuNPs stems from their remarkable optical characteristics and broad applications, particularly in nanomedicine. They have been extensively explored for chemical sensing, biomedical diagnostics, targeted drug delivery, and various pharmaceutical and biomedical domains [79]. These applications leverage the distinctive physicochemical, electrical, and optical attributes of AuNPs, notably their adeptness in absorbing/scattering light across the visible-near infrared (Vis-NIR) spectrum with large optical extinction coefficients. Moreover, AuNPs efficiently convert absorbed optical energy into localized heat, beneficial for ablating nearby cancer cells or pathogenic organisms [79]. Their tunable synthesis and adaptable surface chemistry further increase their appeal. Additionally, AuNPs exhibit significant chemical stability, biocompatibility, and the ability to be quantified and visualized in complex biological settings both in vitro and in vivo. Altogether, these features point to the potential of AuNPs in crafting targeted and effective biomedical systems [80].

Despite their outstanding characteristics, AuNPs face limitations in drug delivery due to the absence of a reservoir or matrix for therapeutics, restricting drug loading primarily to the particle surface. This intrinsic limitation results in a lower loading capacity compared to other nanocarriers (such as lipidic or polymeric carriers) on a weight-per-weight basis [81]. However, AuNPs exhibit remarkable optical and thermal properties, effectively absorbing UV-Vis light with high photothermal conversion efficiency. On the contrary, liposome nanocarriers excel in accommodating therapeutics with ease, achieving acceptable loading capacities and efficiencies. Liposomes, among the earliest FDA-approved nanoparticles (e.g., Doxil in 1995) [82], have served as carriers for various therapeutics in clinical settings. Furthermore, both hydrophilic and hydrophobic drugs find accommodation in the aqueous reservoir or the bilayer membrane of liposomes. Considering the advantageous features of both AuNPs and liposome nanocarriers has gained interest in preparing nanocomposites combining their properties [77].

The potential of AuNP-liposome nanocomposites has been extensively investigated, embedding various types of AuNPs, such as gold nanorods, nanostars, nanoshells, nanospheres, and hollow gold nanoshells, within liposomes for cancer treatment and drug delivery [77]. The choice of excitation wavelength, intensity, and timing of irradiation varies depending on the absorbance band of the AuNPs. Researchers like Lajunen et al. explored light-triggered calcein release using gold nanorods and gold nanostar-embedded liposomes, achieving promising cargo release kinetics within a short span of 5 minutes [83]. Koga et al. demonstrated the release of 80% of cargo within 1 minute using gold nanoshells irradiated with a 660 nm wavelength [80]. In these studies, the mechanism hinges on SPR, leading to a sudden temperature increase in the lipid bilayer, altering membrane fluidity, and triggering cargo release from the liposomes.

Gold nanoparticle loading onto liposomes has been done either by mixing preformed nanoparticles with liposomes or by spontaneous in situ reduction of gold ions by one of the liposome forming components. Often the spontaneous precipitation methods of gold crystallites in liposome/vesicles are practically slow and some of them take days for completion. Furthermore, in such cases the extent of loading and size of the nanoparticles on liposomes cannot be easily manipulated on demand. On the other hand, liposomes have been loaded with nanoparticles by mixing preformed particles with liposomes. In these cases, conventional synthetic strategies are used for the production of gold nanoparticles, e.g. metal ion reduction via Sodium borohydride (NaBH4) or citrate. However, NaBH4 or citrate synthetic protocols are not suitable for particle loading on biofunctional liposomes due to their toxicity and being a strong reducing agent that can modify biological functional groups. Additionally, the high temperature required for the citrate reduction method destroys the liposomes. A summary of the mentioned methods is tabulated in Table 3 which gives information about the AuNP characteristics, nanocomposite synthesis method, and the resultant characteristics of the nanocomposite.

By considering various methods and the adaptability on GUVs, in situ reduction of gold ions on GUVs,

that is proposed by Sau, T.K., et.al., is selected as the gold nanoparticle decorating method for the project. The method is 'green' and efficient and can load liposomes with gold nanoparticles in a simple, rapid, and controlled manner. It allows better control over particle size and number of nanoparticles per liposome as well as their degree of aggregation at the liposome surface. Also, the method uses l-ascorbic acid as the reducing agent which is highly biocompatible. The method involves, solutions of HAuCl4·3H2O and l-ascorbic acid added to the GUV solution. After constant stirring at room temperature for 1 or 2 hours, depending on the HAuCl4·3H2O concentration, the gold nanoparticle coating of GUVs completed.

Table 2.3: Examples of AuNP-liposome nanocomposites [84], [85], [86], [87], [88], [89], [90]

AuNP Characteristics	Preparation Method of Nanocomposite	Nanocomposite Characteristics	Reference
10-50 nm diameter Glycerol as reducing agent	AuNP was covalently immobilized on the thiol-functionalized surface of the liposomes	Size of 190 nm	[84]
Sodium citrate as a reducing agent Functionalized with carboxyl groups	AuNP was covalently linked to the amino-modified liposome surface	Size of 215.2 nm	[85]
Size of 20-40 nm with sodium citrate as a reducing agent	AuNP were noncovalently encapsulated inside liposomes	Size of 60-80 nm	[86]
25 nm PEGylated using Polyethylene glycol Zeta potential of -29.6 mV	Cationic liposomes were decorated using anionic PEGylated AuNP using electrostatic interaction	Size of 180-389 nm Zeta potential of 43-51 mV	[87]
6 nm capped with Cetyltrimethylammonium bromide (CTAB)	Negatively charged liposomes were electrostatically bound to the positive AuNPs	Size of 173 nm Zeta potential of 4.4 mV	[88]
19 nm capped with procyanidin	Negatively charged AuNPs were electrostatically bound to positively charged liposomes	Size of 200-350 nm Zeta potential of -26.01 mV	[89]
Ascorbic acid as a reducing agent	In situ reduction of positive AuNP on the negative liposome surface	Size of 100-150 nm Zeta potential of 20 mV	[90]

In-situ gold nanoparticle reduction on GUVs

The in-situ reduction of gold nanoparticles using $HAuCl_4 \cdot 3H_2O$ (chloroauric acid trihydrate) and l-ascorbic acid is a promising process that involves the transformation of gold ions (Au^{3+}) into elemental gold (Au^0) nanoparticles [91].

To begin, solutions of chloroauric acid and l-ascorbic acid are prepared separately in sucrose solution. Chloroauric acid serves as the source of gold ions, while l-ascorbic acid acts as a reducing agent. When these two solutions are combined, l-ascorbic acid reduces the Au^{3+} ions from the chloroauric acid, resulting in the formation of elemental gold. The chemical reaction is as follows (Eq. 2.9):

$$2HAuCl_4 \cdot 3H_20 + 3C_6H_8O_6 \rightarrow 2Au + 8HCl + 3C_6H_6O_6 + 6H_2O \tag{2.9}$$

In the initial phase of this reaction, small clusters of gold atoms, or nuclei, are formed. This rapid process, known as nucleation, creates numerous tiny gold clusters. Subsequently, additional Au^{3+} ions continue to be reduced and deposited onto these nuclei, allowing the gold nanoparticles to grow in size. The growth phase is influenced by various factors, including the concentration of reactants, temperature, and the presence of stabilizing agents.

For coating GUVs with gold nanoparticles, GUVs are first prepared using methods such as electroformation or gel-assisted swelling. These GUVs, characterized by their single lipid bilayer membrane, are then suspended in a solution containing both chloroauric acid and l-ascorbic acid. Upon adding l-ascorbic acid to the suspension, the reduction process initiates, leading to the nucleation of gold seeds on the GUV surface. This nucleation is facilitated by the interaction of gold ions with the lipid bilayer, aided by surface charges or specific binding sites on the vesicle surface.

Sau et al. [91] studied the impact of the concentration ratio of chloroauric acid and the surface charge of giant unilamellar vesicles (GUVs) on the size of gold nanoparticles formed on GUVs. They found that increasing the concentration of $HAuCl_4$ results in a higher quantity of gold nanoparticles on the GUVs. Additionally, the charge of the lipid dopants significantly influenced the particle loading on the liposomes. Specifically, GUVs doped with cationic lipids had more gold nanoparticles attached compared to those doped with anionic lipids. Although the exact mechanism of gold nanoparticle anchoring to the liposome surface remains unclear, the variation in the number of liposome-anchored nanoparticles based on the lipid dopant suggests that electrostatic interactions might play a role. The ammonium group (>N–(+)) in the lipid molecule may bind to the negatively charged $[AuCl_4]^-$ precursor or negatively charged gold nanoparticles. Furthermore, they observed that at low precursor concentrations, nearly spherical particles formed, while higher precursor concentrations resulted in predominantly non-spherical and aggregated gold nanoparticles. They also noted that larger gold nanoparticles were observed in GUV systems doped with anionic lipids, likely due to different interactions between the dopant lipid and the precursor or gold nanoparticles. Favorable interactions between cationic lipids and the precursor anion $[AuCl_4]^-$ may lead to more nucleation centers on cationic lipid-doped GUVs, unlike in anionic lipid-doped GUVs. Consequently, more nucleation centers result in a higher number of particles with less gold per particle, leading to smaller particles in cationic lipid-doped GUV systems.

3

Materials and methods

3.1. Materials

1,2-dipalmitoyl-sn-glycero-3-phosphocholine (DPPC), 1,2-dioleoyl-sn-glycero-3-phosphocholine (DOPC), and 1,2-distearoyl-sn-glycero-3-phosphoethanolami- ne-N [amino(polyethylene glycol)-2000] (ammonium salt) (DSPE-PEG2000) were purchased from Avanti Polar Lipids (Alabaster, Alabama, US). Atto 488 and Atto 655 were purchased from ATTO-TEC GmbH (Siegen, Germany). Cholesterol with purity of ≥99%, and sulforhodamine B (SRhoB) with 75% dye content, Poly(vinyl alcohol) (PVA) (99% hydrolyzed), Sucrose (≥99.5%), Tris(hydroxymethyl)amino-methane hydrochloride (Tris-HCl), Potassium chloride (KCl), Gold(III) chloride trihydrate (HAuCl4·3H20) (≥99.9% trace metals basis), l-Ascorbic acid (AA) were purchased from Merck Sigma Aldrich (Darmstadt, Germany). Ethanol (EtOH ≥99.8%) was purchased from Honeywell (Charlotte, North Carolina, US). Chloroform (≥99.5%), and tetrahydrofuran (THF, dry) were purchased from Thermo Fisher Scientific (Waltham, Massachusetts, US). MilliQ water was dispensed from Milli-Q IQ 7000 Ultrapure Lab Water System by Merck The HD10.6 line was gifted from Dr.Hsia, Univesity of Maryland.

3.2. Preparation of dye-loaded giant unilamellar vesicles

3.2.1. Synthesis of dye loaded giant unilamellar vesicles

Dye-loaded giant unilamellar vesicles synthesized with minor modifications to the protocol described in Weinberger et al. [33]. Firstly, 200 mOsm sucrose solution in MilliQ water (unbuffered) was used to dissolve the necessary amount of PVA powder to create a 5% (w/v) solution of poly-vinyl alcohol (PVA, 145 kDa, >99% hydrolyzed). After that, this solution was heated on a hot plate to 90°C while being constantly stirred. The solution was allowed to cool to ambient temperature after a few hours. The solution was then filtered using a sterile 200 nm filter (VWR, Amsterdam, the Netherlands) to remove any last bits of undissolved polymer.

To prepare a gel for swelling giant unilamellar vesicles (GUVs), a 24x24 mm coverslip (no.1, Menzel-Glaser) underwent a series of rinses with ethanol, distilled water, and ethanol, followed by blow-drying with nitrogen gas. The coverslip was then treated for 30 seconds with a plasma cleaner (Plasma Prep III, SPI supplies, West Chester, PA, USA) to encourage the gel's adherence to the glass substrate. Subsequently, 100 µL of room temperature PVA solution was spread onto the coverslip, and the glass was tilted to ensure even distribution. A tissue was used to remove any extra solution to guarantee that the thickness of the gel was kept to a minimum. After that, the coverslip was baked at 50 °C for 30 minutes, producing a gel that was clearly solid.

After that, a glass syringe (25 µL, Hamilton) was used to evenly distribute 10 µL of the lipid solution at a concentration of 1 mg/mL in chloroform across the gel surface. Any leftover organic solvent was then allowed to evaporate for half an hour in a vacuum desiccator. After that, the coverslip was placed into a compartmentalized petri dish (4 compartments, VWR, the Netherlands). A Volume of 300 µL of the swelling buffer, which consisted of 200 mOsm sucrose, 10 mM Tris-HCl at pH 7.4, and 5 µM sulforho-

damine B (SRhoB) was carefully applied over the lipid layer. Following a 60-minute incubation period at 50 °C to promote vesicle swelling for DPPC-GUVs and at room temperature for DOPC-GUVs, the vesicles were harvested by gently tilting the petri dish and flushing it once to promote vesicle separation prior to retrieval.

A freezing point osmometer (Osmomat 010, Gonotec, Berlin, Germany) was used to quantify each osmolarity. The osmolarities of the GUV inner and outer solutions matched within a 5 mOsm variation, unless otherwise indicated.

3.2.2. Gold coating of dye-loaded giant unilamellar vesicles

The following methods were employed for growing gold nanoparticles on dye-loaded GUVs based on the protocols described by Hou et.al, [89] and Sau et.al. [91], respectively. For the first formulation, a 0.5 mL solution, containing 200 mOsm sucrose and 2.5 mM HAuCl4, was mixed with 0.5 mL of the dye-loaded GUV solution. To reduce the gold ions, 0.5 mL of another solution containing 2.5 mM l-ascorbic acid (l-AA) and 200 mOsm sucrose was added, and the resulting solution was continuously stirred using a magnetic stirrer. According to the study by Sau et al. [91], for a second formulation, a solution of 0.5 mL containing 200 mOsm sucrose and 5 µM HAuCl4 was combined with 0.5 mL of the dye-loaded GUV solution. To reduce the gold ions, 0.5 mL of a solution containing 8 µM l-AA and 200 mOsm sucrose was added, and the resulting solution was also stirred constantly with a magnetic stirrer. The absorbance of the particle plasmon, indicative of the development of gold nanoparticles, was measured every 30 minutes using the NanoDrop 2000/2000c Spectrophotometer (Thermo Fisher Scientific). The in-situ growth process lasted 2 hours.

3.3. Characterization of giant unilamellar vesicles

3.3.1. Phospholipid content

The amount of phospholipid in the liposome suspension was determined using the Stewart assay. It was discovered that there is a correlation between the lipid concentration and the liposome suspension's absorbance intensity by using the Beer-Lambert law. DPPC standards ranging in concentration from 0.01 to 0.12 mg/mL were dissolved in chloroform and utilized to generate a calibration curve (Fig. C.1). The project's normalization techniques and further computations were based on these calibration curves. In a 15 mL falcon tube, a pre-determined sample amount of sample was mixed with 2 mL of chloroform to determine the phospholipid content of the GUVs. The mixture was vortexed for 30 seconds. The ammonium ferrothicyanate reagent (2 mL) was then added, and the mixture was vigorously vortexed for one minute. Using the Eppendorf Centrifuge 5804/5804R - Benchtop Centrifuge at 2000 RPM for 10 minutes, the organic and aqueous phases were separated. Using a glass pipette, the aqueous phase, where no phospholipids were anticipated, was carefully removed. The Hach Lange DR5000 UV/Vis Spectrophotometer was then used to measure the absorbance intensity of 1 mL of the organic phase that had been transferred to a quartz cuvette at 470 nm. The determined calibration curve was then used to calculate the amount of phospholipid in the liposome suspension.

3.3.2. Fluorescent Microscopy and Image Processing

The Zetasizer Nano ZS, Malvern Panalytical instrument utilized for the Dynamic Light Scattering (DLS) technique has a size constraint, hence size determination was done using ImageJ, an image processing program [43]. To do this, a fluorescent microscope was used to capture photos of the resulting GUVs, which were then processed using ImageJ.

µ-Slide 18 well glass bottom chambered coverslips (ibidi GmbH, Gräfelfing, Germany) were utilized for the GUV imaging. To passivate the glass surface against membrane adhesion, 40 µL of β-casein solution (1 mg/mL, 10 mM Tris-HCl pH 7.4) was added to each well and allowed to rest. The solution was taken out after ten minutes and cleaned with 100 µL of observation buffer (pH 7.4, 205 mOsm glucose, 10 mM tris-HCl). Following the observation buffer wash, 10 µL of GUV solution and 70 µL of observation buffer were added to the well. And waited 10 minutes for the immobilization of GUVs to complete.

A Nikon Exlipse Ti microscope was used to capture the images. It was equipped with a spinning disk confocal module (X-Light, Crest), a digital camera (Orca-Flash 4.0, Hamamatsu), a 100x oil immersion

objective (CFI Plan Apochromat VC, NA 1.40, Nikon), and an LED light source for monochromatic illumination (wavelengths 395/25, 440/20, 470/24, 510/25, 555/15, 575/25, 640/30, Spectra X, Lumencor). The chosen excitation light source wavelength for GUVs labeled with Atto488 was 470 nm, while the wavelength for GUVs labeled with Atto655 was 640 nm. Additionally, micrographs of the dye content are captured utilizing a wavelength of 555 nm for determining the dye content of dye-loaded GUVs.

Size determination

Following the acquisition of the microscope pictures, ImageJ was used to process them. Initially, the 'oval' selection tool was used to choose the GUV on the target image (Fig. A.1a). Next, the pixel area of the GUV of interest is retrieved by choosing 'Measure' from the 'Analyze' menu (Fig. A.1b). Assuming the GUVs are circular and the pixel size of 0.07 µm knowledge within the image, the size of GUV was calculated using the formula given in Section 2.1.3 (Eq. 2.1) To determine the average diameter of the GUV population, the same process was applied to every GUV that was produced using the gel-assisted swelling technique.

Encapsulation efficiency

To assess the encapsulation efficiency of the dye-loaded GUVs, a calibration curve correlating fluorescent intensity with dye concentration was established. Initially, a solution containing 0.008 mg/mL SRhoB dye in a 200 mOsm Sucrose solution was prepared. This solution was then diluted to concentrations of 0.004 mg/mL, 0.002 mg/mL, 0.001 mg/mL, and 0.0005 mg/mL.

Each diluted solution was examined under a fluorescent microscope with a consistent focus on the same z-dimension to maintain uniformity. Fluorescent intensity measurements of the dye solutions at this specific z-dimension were conducted using image processing techniques.

Based on these measurements, a calibration curve was generated plotting dye concentration against fluorescent intensity. This calibration curve provided a quantitative method to determine dye concentrations in subsequent experiments or samples based on their respective fluorescent intensity readings. The resulting calibration curve is depicted in Figure B.1.

To obtain the encapsulation efficiency of GUV, image processing was performed as follows. The 'Area Integrated Density' data for each GUV was acquired using ImageJ's 'Measure' function in order to determine the encapsulation efficiency (Fig. A.1c). The resulting area-integrated density of the GUV was normalized by the background fluorescent intensity in order to obtain the corrected total cell fluorescence (CTCF). Five liposome-free sections of the image are chosen for this purpose, and the mean grey density of their pixels is computed. Following that, the following formula is used to determine the corrected total GUV fluorescence (Eq.3.1). The process is carried out for each GUV on the image, just like in the case of size determination.

$$\begin{aligned}\text{corrected total cell fluorescence} = \text{integrated density of the selected GUV} - \\ (\text{area of the GUV x mean fluorescence of background reading})\end{aligned} \tag{3.1}$$

After determining the CTCF for GUVs, their dye concentrations were calculated by using the calibration curve obtained (Fig. B.1). Then, by using the following equation, their encapsulation efficiency (EE) is calculated as Equation 3.2.

$$\text{EE} = \frac{\text{Dye concentration on GUV}}{\text{Dye concentration of swelling buffer}} \text{x}100\% \tag{3.2}$$

3.4. Stability studies on dye loaded giant unilamellar vesicles

Stability studies on giant unilamellar vesicles (GUVs) involved monitoring changes in their size distribution and encapsulation efficiency under different storage conditions: 4°C, 25°C, and 37°C. Observations were made on the day of synthesis (Day 0) and subsequently every third day over a period of two weeks.

Three coverslips were employed for the experiment, as outlined in Section 3.2.2. Initial images of the GUVs on each coverslip were captured on Day 0. Following this, the GUVs were incubated at the

specified temperatures.

To analyze the data, size distribution and encapsulation efficiency were quantitatively assessed using ImageJ software. Graphical representations of the results were generated to illustrate the changes observed over the experimental period.

3.5. Heat-induced dye release from giant unilamellar vesicles

The experiment aimed to assess the feasibility of thermal dye release using GUVs. Initially, 100 µL samples were heated individually to temperatures of 37°C, 38°C, 39°C, and 40°C. From each temperature condition, an initial sample was collected and placed into the imaging chamber, following the setup detailed in Section 3.3.2. Subsequently, the samples were heated to their respective temperatures, and additional volumes were collected into the imaging chamber.

Fluorescence microscopy images were then acquired to visualize the dye release process. ImageJ software was employed for image processing and analysis, following the methodology outlined in Section 3.3.2. This allowed for the calculation of dye release from the GUVs under varying thermal conditions.

3.6. Giant unilamellar vesicles within the microfluidic platform

Gijs van Veen conducted the design, fabrication, and pressure-induced bursting of GUVs. For detailed procedures, please refer to his master's thesis. Collaborative experiments included studying the effect of syringe introduction of GUVs into the microfluidic system. Two separate imaging wells were prepared according to the protocol outlined in Section 3.3.2. In one well, liposomes were introduced using a pipette, while in the other, a 1 mL syringe was used. Subsequently, fluorescent microscopy images were acquired and analyzed.

4

Results and discussion

Throughout the project, dye-loaded GUVs were synthesized using the gel-assisted swelling method by incorporating dye into the swelling buffer. The characterization was performed through image processing of fluorescent microscopy images. An attempt was made to coat these dye-loaded GUVs with gold nanoparticles by in-situ reduction of gold nanoparticles using l-ascorbic acid as the reducing agent. However, since the UV/Vis absorbance measurements did not possess gold nanoparticle coating of GUVs, the thermal-induced release of cargo from GUVs via bulk heating was conducted to evaluate the proposed mechanism for future studies. This chapter presents the results and observations obtained from the project.

4.1. Synthesis and characterization of giant unilamellar vesicles

Throughout the project, liposomes were synthesized using the gel-assisted swelling method. The initial aim was to produce 1,2-dipalmitoyl-sn-glycero-3-phosphocholine (DPPC) liposomes with 0.1% fluorescent lipid included in the formulation. DPPC was selected because its phase transition temperature (T_m = 41°C) is slightly above body temperature, ensuring safety as it does not cause thermal damage to body tissues. This high transition temperature ensures that the lipid bilayer remains in an ordered gel phase below T_m and shifts to a disordered liquid phase at higher temperatures, enabling cargo release.

According to Weinberger et al. [33], successful swelling of DPPC liposomes occurs at 50°C. To synthesize DPPC liposomes, a glass coverslip was coated with PVA gel after UV/Ozone treatment. After baking the PVA gel for 30 minutes, 10 µL of 1 mg/mL DPPC:Atto655 (99.9:0.1) was spread on the coverslip. After evaporating the organic solvent (chloroform) in a desiccator for 30 minutes, 300 µL of swelling buffer (200 mOsm sucrose, 10 mM Tris-HCl, pH 7.4) was added to the coverslip, which was then placed in a 50°C oven. After an hour, the GUVs were collected and observed under a fluorescent microscope. To ensure any synthesis issues were due to the lipid formulation, a control group of DOPC-GUVs was synthesized following the same steps, with a lipid composition of DOPC:Atto655 (99.9:0.1). The control group yielded over 1000 GUVs/300 µL, with an average size of 7.65 ± 3.46 µm, indicating successful synthesis. However, DPPC liposomes had a low yield (< 100 GUVs/300 µL), were smaller (4.35 ± 2.89 µm), and tended to cluster.

To optimize DPPC-GUV synthesis, another study by Haluska et al. [92] was reviewed, which found successful DPPC-GUV synthesis using the electroformation method at 60°C. Repeating the synthesis at 60°C did not yield different results from the 50°C synthesis. It was concluded that DPPC-GUV synthesis is only successful at temperatures above its phase transition temperature of 41°C. However, the DPPC-GUVs obtained were unsuitable for this project due to their low yield, small size (smaller than the microfluidic platform's minimum nozzle dimension of 4x4 µm with a 5° angle), and clustering. Since the primary goal was to observe dye release within the microfluidic platform, DPPC-GUVs were deemed unfavorable for integration. Therefore, DOPC-GUVs were used for the remainder of the project.

The Stewart assay, a common method for characterizing and standardizing liposomal drug formulations

for small unilamellar vesicles (SUVs) and large unilamellar vesicles (LUVs), was adapted for giant unilamellar vesicles (GUVs). The protocol outlined in Section 3.3.1 was followed. Due to the relatively low theoretical lipid content for gel-swelled GUVs (0.067 mg/mL) compared to SUVs and LUVs produced by the thin-film hydration method (approximately 20 mg/mL), the amount of DOPC-GUV sample added to chloroform required optimization. Different volumes (10, 20, 50, 100, and 200 µL) of GUV samples were prepared and dissolved in 2 mL of chloroform. After adding ammonium ferrothiocyanate reagent and centrifuging for phase separation, the absorbance was measured using a UV/Vis spectrophotometer. The absorbance data were then processed using a calibration curve for DOPC. Due to the low phospholipid content of GUVs, this method did not yield reliable results. A more detailed explanation is provided in Appendix D.

4.2. Synthesis and characterization of dye-loaded giant unilamellar vesicles

By adding dye to the swelling buffer, the gel-assisted swelling synthesis method's dye loading of the GUVs was carried out. To determine how dye affects the yield of dye-loaded GUVs, three different dye concentrations, 5 µM, 1.7 mM, and 17 mM, have been explored. As the dye concentration increases, the number of successfully synthesized GUVs significantly decreases. As well as, a higher proportion of the GUVs appeared empty, indicating a lack of dye encapsulation, especially at higher dye concentrations.

Obtaining lower amounts of GUVs and reduced encapsulation efficiency can be due to several factors, including osmotic pressure and membrane stress, solubility and precipitation of the dye, and lipid-dye interactions. For higher dye concentrations, significant osmotic pressure differences arise between the interior and exterior of the forming vesicles. This imbalance can stress the lipid bilayer during formation and cause vesicle rupture or incomplete formation.

Regarding solubility and precipitation, high dye concentrations may cause the dye to precipitate out of the solution, leading to poor encapsulation. This results in fewer successfully formed GUVs and many appearing empty because the dye is not in a suitable state for encapsulation. The solubility of the dye in the swelling buffer that is used for hydrating the lipids may be exceeded at higher concentrations, causing aggregation and precipitation of dye and disrupting vesicle formation.

And for the lipid-dye interactions, high dye concentrations may interact unfavorably with lipid molecules, disrupting the self-assembly process necessary for GUV formation. This can lead to fewer vesicles being formed and empty vesicles. Strong binding of the dye to lipids can interfere with normal bilayer formation, resulting in defects or instability in the forming vesicles. Additionally, high dye concentrations can cause steric hindrance, which means, the space within the forming vesicles becomes too crowded, preventing effective encapsulation of dye within vesicles.

The results indicate that higher concentrations of dye negatively impact both the formation and encapsulation efficiency of DOPC-based GUVs. The primary reasons of this observation include osmotic pressure imbalances, steric interactions, solubility issues, and unfavorable interactions between the dye and lipid molecules. For optimal GUV synthesis and dye encapsulation, maintaining a lower dye concentration (such as 5 µM) is recommended, as it minimizes osmotic stress and other disruptive effects, leading to more successful vesicle formation and encapsulation. So, for the remainder of the project, 5 µM was determined to be the optimal concentration to produce a sizable number of dye-loaded GUVs.

Figure 4.1 displays the microscope pictures of the dye-loaded GUVs that were obtained. It is possible to see distinct sections of the GUVs together or separately by stimulating different light sources. For instance, 4.1a depicts the image of the GUVs' lipid membrane since just one excitation wavelength, 640 nm (5% intensity), is chosen, and this wavelength is appropriate for excitation of the dye-fluorescent labeling lipid (DOPE-Atto655). However, as Figure 4.1b is activated with a light source of 555 nm (5% intensity) that is appropriate for the excitation wavelength of the dye used (Sulforhodamine B), it only displays the dye content within GUVs. Additionally, both of these wavelengths might be used to

stimulate GUVs, which would display the lipid membrane as well as dye encapsulated (Fig. 4.1c).

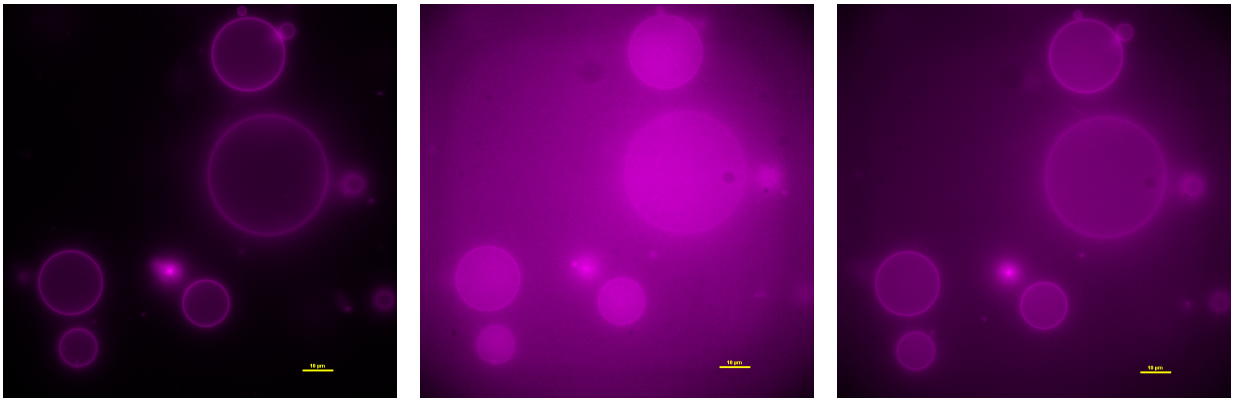

(a) Lipid Only **(b)** Dye Only **(c)** Lipid and Dye

Figure 4.1: Fluorescent micrographs of dye-loaded GUVs. (a) Only the lipid dye is excited (640 nm, 5% intensity). (b) Only the encapsulated dye is excited (555 nm, 5% intensity). (c) Both the lipid dye and encapsulated dye are excited (640 nm, 555 nm, 5% intensity). The scale bar is 10 µm in all images.

The method used for determining dye encapsulation efficiency in small unilamellar vesicles (SUVs) involves measuring the UV/Vis absorbance of the encapsulated dye after overnight dialysis. However, this method proved unsuitable for giant unilamellar vesicles (GUVs) for several reasons.

Firstly, it was observed that when GUVs were subjected to dialysis, the remaining volume after dialysis was significantly reduced to 45 µL from the initial 800 µL. This considerable volume loss suggests that most of the sample volume post-swelling consisted of a blank swelling buffer, resulting in a very low number of liposomes. This observation corroborates the findings from the previous section (Section 4.1). Consequently, due to the low number of GUVs, the sample after dialysis appeared transparent, making it impossible to detect the intended color change necessary for UV/Vis absorbance measurement after GUV lysis.

To address the possibility that dialysis might induce GUV instability and subsequent dye release, dialyzed GUVs were imaged. The imaging results indicated that dialysis did not cause instability or dye release from the lipid bilayer, as the encapsulation efficiency was similar to that of the non-dialyzed sample. This finding implies that, like the Stewart Assay, the limited quantity of GUVs hindered the effectiveness of the conventional encapsulation efficiency method.

Given these challenges, an alternative approach using image processing was employed to determine the encapsulation efficiency of GUVs. This method proved to be more suitable, providing reliable measurements despite the low number of vesicles and avoiding the issues associated with the UV/Vis absorbance method post-dialysis.

4.3. Effect of lipid compositions on GUV stability

The sub-research question of the thesis has been addressed by examining the stability of GUVs at various temperatures and lipid compositions. To do this, sizes and dye encapsulation efficiencies of GUVs were measured on the day of synthesis, the following day, and then every third day over the following two weeks. Three separate 18-well glass bottom chambered coverslips have been prepared for characterization. To learn about the stability of GUVs in the refrigerator, at room temperature, and body temperature, each of these coverslips was incubated at 4 °C, 25 °C, and 37 °C, respectively.

The lipid compositions that have been used for stability study and their molar ratios are given in Table 4.1. Within these lipid formulations, we were not able to successfully synthesize DOPC:Chol:DSPE-PEG2000:Atto655 GUVs whereas all other formulations were successfully synthized. As a result, no further size and dye encapsulation check has been made for this liposome formulation.

Table 4.1: Lipid compositions used for stability study

Lipid Composition	Molar Ratio (%)
DOPC:Atto655	99.9:0.1
DOPC:Chol:Atto655	79.9:20:0.1
DOPC:DSPE-PEG2000:Atto655	94.9:5:0.1
DOPC:Chol:DSPE-PEG2000:Atto655	74.9:20:5:0.1

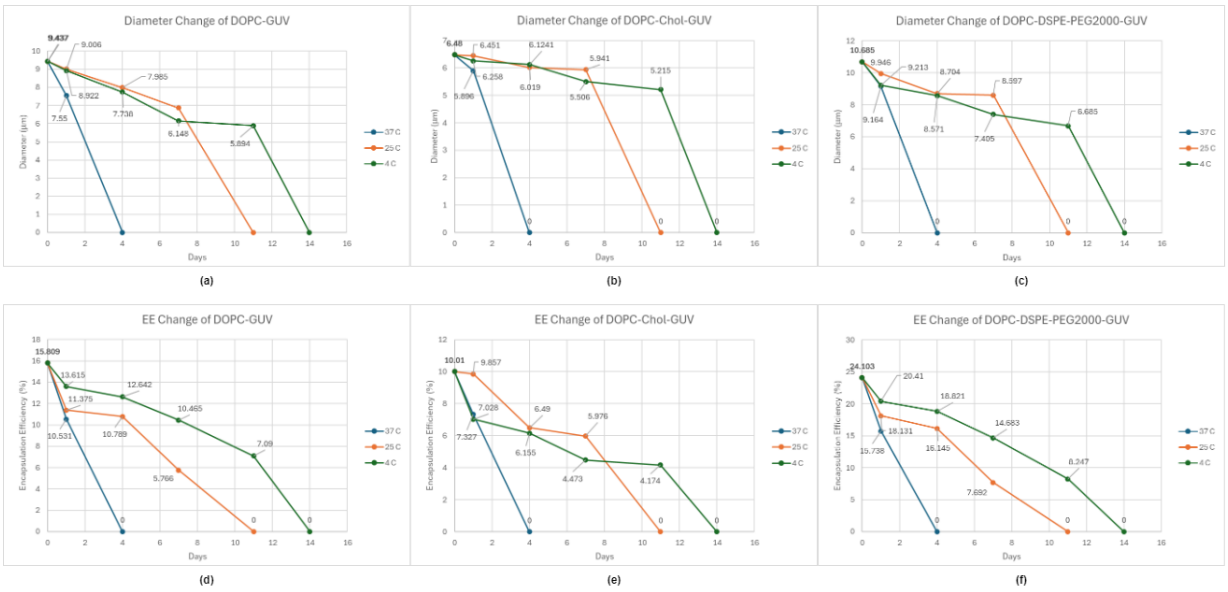

Figure 4.2: Diameter change and encapsulation efficiency results of 2-week stability study, (a) diameter change of DOPC-GUV for 4, 25 and 37 °C, (b) diameter change of DOPC-Chol-GUV for 4, 25 and 37 °C, (c) diameter change of DOPC-DSPE-PEG2000-GUV for 4, 25 and 37 °C, (d) encapsulation efficiency change of DOPC-GUV for 4, 25 and 37 °C, (e) encapsulation efficiency change of DOPC-Chol-GUV for 4, 25 and 37 °C, (f) encapsulation efficiency change of DOPC-DSPE-PEG2000-GUV for 4, 25 and 37 °C.

The results of the stability study are given in Figure 4.2 in terms of diameter change and encapsulation efficiency of different lipid compositions at 3 different temperatures. As it can be observed from Figure 4.2a and 4.2d, liposomes have an initial average diameter of 9.437 µm and it decreases to 5.094 µm on the 11th day at 4 °C and 6.867 µm on the seventh day at 25 °C and 7.55 micrometer at the 1st day at 37 °C. Also, GUVs at 37 °C can only survive up to 4 days, at 25 °C GUVs can survive up to 11 days, and at 4 °C can survive up to 14 days. For their encapsulation efficiency, DOPC-GUVs, liposomes have an initial encapsulation efficiency of 15.809% and it decreases to 7.09% on the 11th day at 4 °C and 5.766% on the seventh day at 25 °C and 7.55% at the 1st day at 37 °C. The data indicates that DOPC-GUVs exhibit significant size reduction and loss of encapsulation efficiency over time, particularly at higher temperatures. At 37°C, the rapid decrease in diameter and encapsulation efficiency suggests that the GUVs are less stable, likely due to increased lipid fluidity at elevated temperatures. The relatively better stability at 4°C can be a result of the reduced kinetic energy, resulting in slower degradation processes on liposomes.

For DOPC:Chol GUVs, liposomes have an initial average diameter of 6.48 µm and it decreases to 5.215 µm on the 11th day at 4 °C and 5.506 µm on the seventh day at 25 °C and 5.896 µm at the 1st day at 37 °C. For their encapsulation efficiency, DOPC-GUVs, liposomes have initial encapsulation efficiency of 10.01% and it decreases to 4.174% on the 11th day at 4 °C and 4.473% on the seventh day at 25 °C and 7.327 on the 1st day at 37 °C. The inclusion of cholesterol in the lipid composition appears to confer some stabilization to the GUVs, as seen by the relatively smaller decrease in diameter and encapsulation efficiency compared to DOPC-GUVs. Cholesterol is known to stabilize lipid bilayers by reducing bilayer fluidity and increasing its thickness, which can enhance vesicle stability in terms of encapsulation of the cargo [93].

For DOPC:DSPE-PEG2000 GUVs, liposomes have an initial average diameter of 10.685 µm and it decreases to 6.685 µm on the 11th day at 4 °C and 8.579 µm on the seventh day at 25 °C and 9.164 µm at the 1st day at 37 °C. For their encapsulation efficiency, DOPC:DSPE-PEG2000-GUVs, liposomes have an initial encapsulation efficiency of 24.103% and it decreases to 8.247% on the 11th day at 4C and 7.692% on the seventh day at 25 °C and 15.738 on the 1st day at 37 °C. The addition of DSPE-PEG2000 significantly improves the initial encapsulation efficiency of the GUVs. PEGylation of the liposomes enhances stability by providing a steric barrier that reduces interactions with other vesicles. This is evidenced by the highest initial encapsulation efficiency among the three compositions and a relatively moderate decrease over time. However, temperature still plays a critical role in stability even with the PEGylation.

These results show, all GUV compositions show improved stability at lower temperatures. At 4°C, vesicles maintain a larger diameter and higher encapsulation efficiency for a longer period. At 37°C, GUVs are less stable, with significant decreases in diameter and encapsulation efficiency, indicating increased lipid bilayer fluidity and faster degradation rates. Additionally, DOPC:Chol demonstrates improved stability compared to pure DOPC-GUVs, suggesting cholesterol's role in enhancing bilayer rigidity and reducing permeability. Also, DOPC:DSPE-PEG2000 shows the highest initial encapsulation efficiency and moderate decreases over time, highlighting the stabilizing effect of PEGylation. This composition also maintains larger diameters at 37°C compared to bare DOPC-GUVs and DOPC:Chol-GUVs, indicating better thermal stability.

In conclusion, the study reveals that both temperature and lipid composition are critical factors affecting the stability of GUVs. Lower temperatures generally enhance vesicle stability, while certain lipid modifications, such as the inclusion of cholesterol and/or PEGylation, can further improve the longevity and encapsulation efficiency of the GUVs.

4.4. Synthesis and characterization of gold-nanoparticle coated giant unilamellar vesicles

Based on the literature, two different gold nanoparticle coating experiments have been performed. In the first formulation, 500 µL GUV solution was added to 500 µL of 2.5 mM HAuCl4·3H2O and 500 µL of 2.5 mM l-ascorbic acid solution and constantly stirred for 2 hours [89]. Whereas for the second formulation, 500 µL GUV solution has been added to 500 µL of 5 µM HAuCl4·3H2O and 500 µL of 8 µM l-ascorbic acid solution and constantly stirred for 2 hours [91]. The obtained solutions of gold-nanoparticle coated GUVs have been characterized by fluorescent microscopy and UV/Vis absorbance measurements which is presented in Figure 4.3 and Figure 4.4, respectively.

So for the first formulation, fluorescent microscopy showed black aggregates (Fig.4.3a), potentially gold particles, and very few GUVs. And UV/Vis absorbance measurement (Fig.4.4 - dark blue line) showed high absorbance peaks, indicating the presence of nanoparticles. Whereas for the second formulation, fluorescent microscopy (Fig.4.3a) showed very few GUVs and no black aggregates. UV/Vis absorbance (Fig.4.4 - orange line) showed lower absorbance peaks compared to the first formulation. UV/Vis absorbance measurement of non-coated GUVs (Fig.4.4 - green line) showed baseline absorbance, confirming the absence of gold nanoparticles.

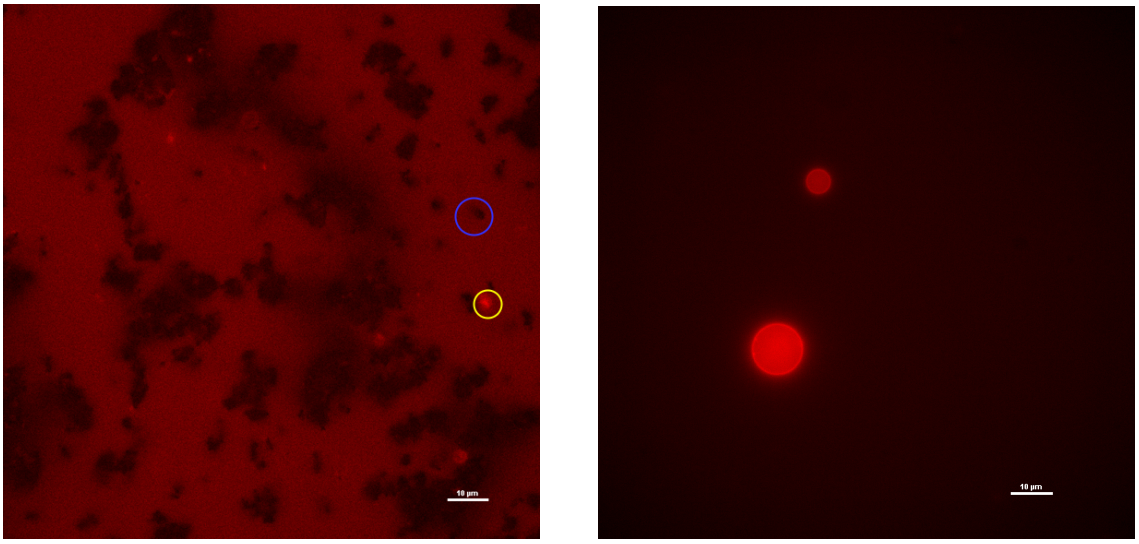

(a) Synthesis with 2.5 mM HAuCl4·3H2O and 2.5 mM l-ascorbic acid

(b) Synthesis with 5 µM HAuCl4·3H2O and 8 µM l-Ascorbic Acid

Figure 4.3: Fluorescent micrographs of gold nanoparticle coating of GUVs. Both the lipid dye and encapsulated dye are excited in both images (640 nm, 555 nm, 5% intensity) (a) Synthesis with 2.5 mM HAuCl4·3H2O and 2.5 mM l-Ascorbic Acid. Blue circle indicates possible gold nanoparticle aggregates, yellow circle indicates DOPC-GUV. (b) Synthesis with 5 µM HAuCl4·3H2O and 8 µM l-Ascorbic Acid. The scale bar is 10 µm in all images.

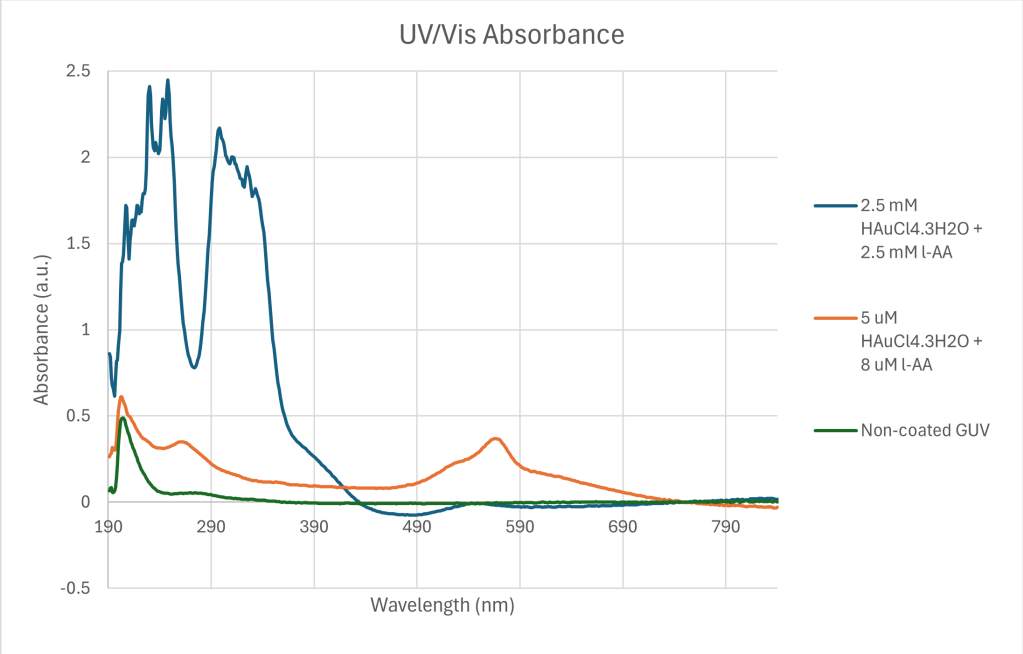

Figure 4.4: Fluorescent microscopy images of gold-coating experiment of DOPC-GUV, blue circle indicates possible gold nanoparticle, yellow circle indicates DOPC-GUV. Scale bar is 10 µm.

In the first formulation, due to the high concentration of HAuCl4.3H2O (2.5 mM) and l-ascorbic acid (2.5 mM) likely led to rapid reduction and nucleation of gold particles, resulting in large aggregates. These aggregates are visible as black spots under the fluorescent microscope. The large aggregates might be too big to coat the GUVs efficiently, thus leading to a low number of observed coated GUVs. Whereas in the second formulation, the lower concentrations of HAuCl4.3H2O (5 µM) and l-ascorbic acid (8 µM) may have resulted in insufficient nucleation and growth of gold nanoparticles. This could explain the absence of black aggregates and the low UV/Vis absorbance peaks. The loss of GUVs through the in-situ growth process suggests that the conditions were not optimal for efficient AuNP

formation and subsequent coating. Successful coating of GUVs with AuNPs requires nanoparticles of appropriate size and distribution.

To overcome these issues, the reduction reaction could be performed at a slower rate, possibly by adjusting the temperature or using a controlled addition of the reducing agent, to control the size and distribution of AuNPs. As well as modifying the GUV surface with thiol groups or other ligands that have a high affinity for gold, facilitating better binding and coating of the nanoparticles. Finally, to better characterize the size and distribution of AuNPs coated on the GUVs, dynamic light scattering (DLS) and transmission electron microscopy (TEM) can be used.

In conclusion, the gold nanoparticle coating of GUVs was unsuccessful due to issues related to nanoparticle aggregation and insufficient formation. To achieve a better coating of GUVs, the concentrations of the reagents should be optimized, reduction process should be performed more controlled, and GUV surface could potentially be functionalized. Future experiments should focus on these adjustments to improve the efficiency of GUV coating with gold nanoparticles.

4.5. Heat-induced dye release from giant unilamellar vesicles

In this experiment, DOPC-based giant unilamellar vesicles (GUVs) were incubated at temperatures of 37°C, 38°C, 39°C, 40°C, and 41°C for an hour, and their resulting encapsulation efficiencies have been checked to observe any dye release due to bulk heating from the vesicles. The encapsulation efficiency of the GUVs was measured at each temperature, yielding the following results (Fig.4.5):

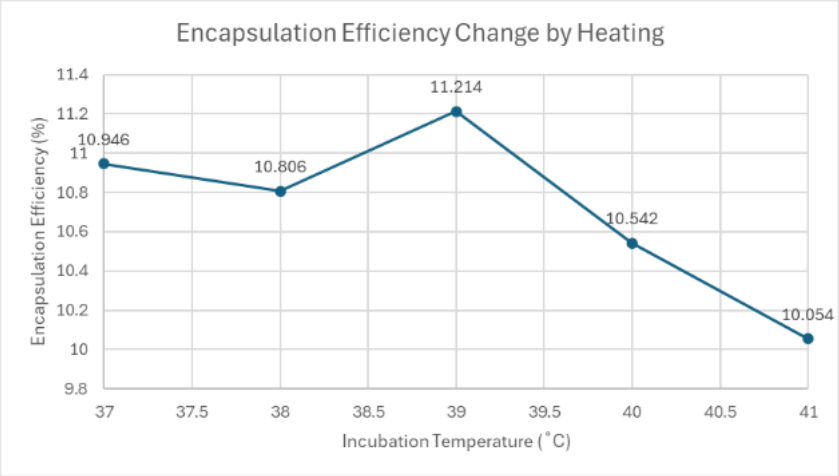

Figure 4.5: Encapsulation efficiency change of DOPC-GUV after incubation for an hour at 37, 38, 39, 40, and 41 °C

As can be seen in Figure 4.5, The encapsulation efficiency remains relatively stable between 37°C and 39°C. The slight increase at 39°C (11.214%) can be a result of experimental variability, but it suggests that within this range, the GUVs maintain their structural integrity and encapsulation efficiency effectively. At 40°C and 41°C, the encapsulation efficiency begins to decline (10.542% and 10.054%, respectively). This suggests that as the temperature increases beyond 39°C, the stability of the vesicles is compromised, resulting in increased dye release.

Since the phase transition temperature of DOPC is much lower than the experimental temperatures, the vesicles remain in the liquid crystalline phase throughout the experiment. However, even within the liquid crystalline phase, higher temperatures can increase the fluidity and permeability of the lipid bilayer. At temperatures above 39°C, the kinetic energy of the lipid molecules increases which can cause greater bilayer permeability [94]. This increased permeability likely leads to the observed decrease in encapsulation efficiency, as the dye molecules can get released from the vesicles. Higher temperatures can also affect the overall structural integrity of the GUVs. As the temperature rises, vesicle fusion or leakage increases, further contributing to the reduced encapsulation efficiency observed at 40°C and 41°C.

To conclude, the results of the bulk-heating induced dye release experiment indicate that DOPC-based GUVs maintain relatively stable encapsulation efficiency up to 39°C. Beyond this temperature, there is a decline in encapsulation efficiency, likely due to increased membrane fluidity and permeability, and potentially compromised vesicle integrity. This behavior is consistent with the properties of DOPC, which remains in the liquid crystalline phase at these temperatures but exhibits increased instability and leakage at higher temperatures. These findings suggest that in the case of successful gold nanoparticle coating of DOPC-GUVs, light-induced dye release due to the surface plasmon resonance effect can be achieved.

4.6. Giant unilamellar vesicles within microfluidic platform

In this study, the impact of different methods for introducing giant unilamellar vesicles (GUVs) into a microfluidic platform was discovered, specifically comparing the use of a pipette versus a syringe. The objective was to determine how these introduction methods affect the number of GUVs present and their encapsulation efficiency within the microfluidic environment. The resulting fluorescent micrographs have been presented in Figure 4.6.

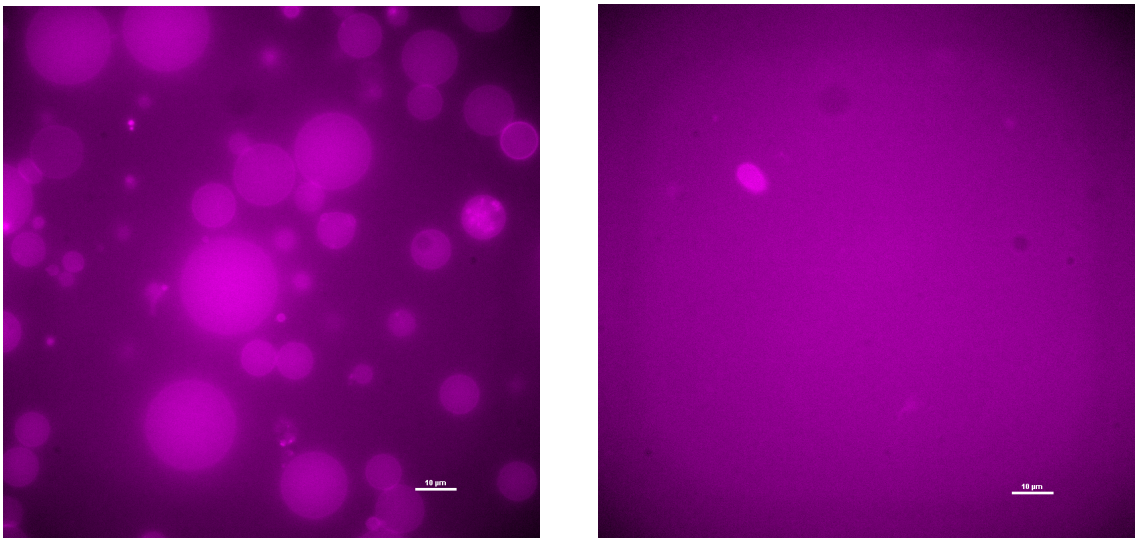

(a) By pipette **(b)** By syringe

Figure 4.6: Fluorescent micrographs of different techniques for GUV introduction. Only encapsulated dye is excited in both images (555 nm, 5% intensity). (a) GUVs introduced by pipette (b) GUVs introduced by syringe. The scale bar is 10 µm in all images.

Initially, GUVs were introduced into the microfluidic system using two distinct methods, pipetting, and syringing, and subsequent analysis revealed distinct outcomes for each method. When GUVs were introduced via a pipette, a higher number of intact vesicles were observed (Fig. 4.6a). These GUVs exhibited notably higher encapsulation efficiency, indicating successful loading of the internal cargo with minimal leakage or disruption during the introduction process. This observation suggests that the gentle handling afforded by the pipette minimizes mechanical stress on the liposomes, preserving their structural integrity and functional capacity to encapsulate dye.

Conversely, when GUVs were introduced using a syringe, a noticeable decrease in the number of intact vesicles was observed (Fig. 4.6b). This decrease correlated with a higher background fluorescent intensity, indicative of compromised vesicle integrity and potential leakage of encapsulated dye. The higher background fluorescence suggests the presence of dispersed dye molecules, possibly due to ruptured vesicles during the more forceful introduction via the syringe.

The observed differences between the pipette and syringe methods can be attributed to several factors. The pipette allows for a more controlled and gentle introduction of GUVs, minimizing shear forces and

mechanical stress that could lead to vesicle rupture. In contrast, the syringe exerts greater pressure during injection, potentially causing physical damage to the fragile vesicles and resulting in lower retention rates and compromised encapsulation efficiency.

These findings underscore the importance of methodological considerations in microfluidic-based studies involving lipid vesicles. Opting for gentle handling techniques, such as pipetting, can enhance experimental outcomes by preserving vesicle integrity and maximizing encapsulation efficiency.

In conclusion, the choice of introduction method significantly influences the behavior and succession of GUVs within microfluidic platforms. By selecting appropriate introduction techniques, researchers can optimize experimental conditions to maximize the efficacy of drug delivery systems based on lipid vesicles.

5

Conclusion

Important knowledge regarding the synthesis, characterization, and use of giant unilamellar vesicles as drug-carrying agents was acquired through the master's thesis project. The aim was to produce DPPC-GUVs by using the gel-assisted swelling method. The success of the synthesis was not as high as anticipated, even with the use of the documented methodologies. Because of its lower yield, smaller size, and clustering, DPPC may not be appropriate for the suggested drug delivery method, on the other hand, the control group of DOPC-GUVs produced a noticeably higher number of vesicles. In adapting the Stewart assay for GUVs to characterize their phospholipid content, significant variability was found, highlighting the assay's unsuitability for low-concentration of GUVs due to differences in yield compared to SUVs and LUVs.

Investigating dye encapsulation in GUVs showed that greater dye concentrations had an adverse effect on the synthesis and encapsulation of dye. These results could have been caused by osmotic pressure, solubility of dye, and interactions between the dye and lipid at high dye concentrations. Therefore, it was shown that in order to produce a significant number of dye-loaded GUVs, a lower dye concentration of 5 µM was ideal.

Additionally, stability research revealed that, especially at higher temperatures, GUVs show a noticeable decrease in size and encapsulation efficiency over time. The formulations of DOPC-GUVs, DOPC-Chol, and DOPC-DSPE-PEG2000 showed differing levels of stability; PEGylation offered the best initial encapsulation efficiency and enhanced thermal stability. While cholesterol and PEGylation further increased the GUVs' lifetime and encapsulation efficiency, as well as lower temperatures generally improved vesicle stability.

Attempts to coat GUVs with gold nanoparticles highlighted the challenges of nanoparticle aggregation and insufficient formation. While lower concentrations of HAuCl4·3H2O and ascorbic acid failed to form enough nanoparticles, higher amounts produced large aggregates that were unsuitable for coating. These results imply that coating efficiency could be increased by adjusting reagent concentrations, managing the reduction process, and maybe functionalizing the GUV surface.

It was discovered that DOPC-GUVs retain a comparatively consistent encapsulation efficiency up to 39°C, with a reduction at higher temperatures, while evaluating dye release caused by bulk heating. Increased membrane fluidity and permeability are probably the cause of these observations, highlighting the possibility of surface plasmon resonance-induced dye release in gold nanoparticle-coated GUVs in future studies.

Lastly, an analysis was conducted on the effects of two different techniques for integrating GUVs into a microfluidic platform. Comparing the effect of the pipette and a syringe, which increased vesicle rupture and leakage, revealed that pipetting introduces more intact vesicles and improved encapsulation efficiency. This highlights how crucial it is to handle vesicles gently when conducting microfluidic research

to maintain vesicle integrity.

All things considered, this effort has offered a thorough understanding of the synthesis, stability, and optimization of GUVs for drug-delivery studies in addition to useful advice on how to handle and use them in microfluidic platforms. These discoveries advance our knowledge of the behavior of lipid vesicles and open the door to possible advancements in drug delivery technologies.

6

Future recommendations

To improve the efficacy of giant unilamellar vesicles in drug delivery applications, future researches should focus on perfecting their manufacture and use. In light of the difficulties associated with DPPC liposomes, additional research into substitute phospholipids or hybrid lipid compositions may produce more effective techniques. The production and quality of DPPC-GUVs may be increased by looking into alternative GUV synthesis methods or by making changes to current protocols, such as changing the lipid concentration adding stabilizing agents, or using different synthesis techniques.

It is necessary to develop or improve alternative characterization techniques to overcome the variability in the Stewart assay for GUVs. It is critical to develop methods for measuring phospholipid content at low concentrations with accuracy and little variability. Employing sophisticated analytical instruments such as mass spectrometry or high-performance liquid chromatography (HPLC) may yield more dependable outcomes and enable a more comprehensive understanding of GUV composition.

The encapsulation efficiency and stability of GUVs at higher dye concentrations need to be systematically studied. Investigating the interaction between lipids and different types of dyes, including their chemical properties and potential modifications, could lead to improved encapsulation of cargo.

The stability issues that have been reported over time, especially at high temperatures, point to the necessity for more research into lipid compositions to improve thermal stability. Different lipid types with higher phase transition temperature, such DPPC, may be studied, or new PEGylated lipids or cholesterol derivatives may be added as stabilizing molecules to help create more stable vesicles.

Another crucial topic is improving the gold nanoparticle coating of GUVs. Preventing aggregation and improving the coating efficiency of gold nanoparticles may be achieved by optimizing the reagent concentration and the nanoparticle synthesis conditions. Investigating surface functionalization methods, such as utilizing linker molecules or particular ligand attachment, may enhance the adherence of nanoparticles to the GUV surface.

More research is necessary to determine whether surface plasmon resonance in gold-coated GUVs can cause dye release in response to light. Precise control over dye release may result from in-depth research on the relationship between light and the coated vesicles, taking into account the effects of different light intensities and wavelengths. It would be crucial to determine the biocompatibility of GUVs and possible toxicity in cellular or in vivo models before using them in drug delivery systems.

Lastly, to ensure vesicle integrity, the processes for introducing GUVs into microfluidic substrates must be optimized. Vesicle rupture and leakage can be minimized by developing gentle handling techniques and optimizing microfluidic devices to accommodate the fragility of GUVs. Investigating different vesicle insertion techniques, such as automated dispensing systems or microinjectors, may enhance the uniformity and effectiveness of test sets.

All things considered, the knowledge acquired from this effort emphasizes how critical it is to keep improving giant unilamellar vesicle synthesis and characterization techniques. Future research can further advance liposome-based drug delivery systems by resolving the existing constraints and investigating novel ways.

Bibliography

[1] Graeme J. Hankey. “Stroke”. English. In: *The Lancet* 389.10069 (Feb. 2017). Publisher: Elsevier, pp. 641–654. ISSN: 0140-6736, 1474-547X. DOI: 10.1016/S0140-6736(16)30962-X. URL: https://www.thelancet.com/journals/lancet/article/PIIS0140-6736(16)30962-X/fulltext.

[2] Catherine Owens Johnson et al. “Global, regional, and national burden of stroke, 1990–2016: a systematic analysis for the Global Burden of Disease Study 2016”. en. In: *The Lancet Neurology* 18.5 (May 2019), pp. 439–458. ISSN: 14744422. DOI: 10.1016/S1474-4422(19)30034-1. URL: https://linkinghub.elsevier.com/retrieve/pii/S1474442219300341.

[3] M. Budai and M. Szógyi. “[Liposomes as drug carrier systems. Preparation, classification and therapeutic advantages of liposomes]”. hun. In: *Acta Pharmaceutica Hungarica* 71.1 (2001), pp. 114–118. ISSN: 0001-6659.

[4] Michael S. Rafii and Argye E. Hillis. “Compendium of cerebrovascular diseases”. In: *International Review of Psychiatry* 18.5 (Jan. 2006). Publisher: Taylor & Francis, pp. 395–407. ISSN: 0954-0261. DOI: 10.1080/09540260600935405. URL: https://doi.org/10.1080/09540260600935405.

[5] Charlotte Rosso et al. “Hyperglycaemia, Insulin Therapy and Critical Penumbral Regions for Prognosis in Acute Stroke: Further Insights from the INSULINFARCT Trial”. en. In: *PLOS ONE* 10.3 (Mar. 2015). Publisher: Public Library of Science, e0120230. ISSN: 1932-6203. DOI: 10.1371/journal.pone.0120230. URL: https://journals.plos.org/plosone/article?id=10.1371/journal.pone.0120230.

[6] R. Brouns and P. P. De Deyn. “The complexity of neurobiological processes in acute ischemic stroke”. In: *Clinical Neurology and Neurosurgery* 111.6 (July 2009), pp. 483–495. ISSN: 0303-8467. DOI: 10.1016/j.clineuro.2009.04.001. URL: https://www.sciencedirect.com/science/article/pii/S0303846709000821.

[7] Craig S. Anderson et al. “Low-Dose versus Standard-Dose Intravenous Alteplase in Acute Ischemic Stroke”. In: *New England Journal of Medicine* 374.24 (June 2016). Publisher: Massachusetts Medical Society, pp. 2313–2323. ISSN: 0028-4793. DOI: 10.1056/NEJMoa1515510. URL: https://doi.org/10.1056/NEJMoa1515510.

[8] Götz Thomalla et al. “MRI-Guided Thrombolysis for Stroke with Unknown Time of Onset”. In: *New England Journal of Medicine* 379.7 (Aug. 2018). Publisher: Massachusetts Medical Society, pp. 611–622. ISSN: 0028-4793. DOI: 10.1056/NEJMoa1804355. URL: https://doi.org/10.1056/NEJMoa1804355.

[9] Michael A. Moskowitz, Eng H. Lo, and Costantino Iadecola. “The Science of Stroke: Mechanisms in Search of Treatments”. In: *Neuron* 67.2 (July 2010), pp. 181–198. ISSN: 0896-6273. DOI: 10.1016/j.neuron.2010.07.002. URL: https://www.sciencedirect.com/science/article/pii/S0896627310005404.

[10] Giuseppina Bozzuto and Agnese Molinari. “Liposomes as nanomedical devices”. English. In: *International Journal of Nanomedicine* 10.1 (Feb. 2015). Publisher: Dove Press, pp. 975–999. DOI: 10.2147/IJN.S68861. URL: https://www.dovepress.com/liposomes-as-nanomedical-devices-peer-reviewed-fulltext-article-IJN.

[11] Haojie Wang et al. “Liposomal 9-Aminoacridine for Treatment of Ischemic Stroke: From Drug Discovery to Drug Delivery”. In: *Nano Letters* 20.3 (Mar. 2020). Publisher: American Chemical Society, pp. 1542–1551. ISSN: 1530-6984. DOI: 10.1021/acs.nanolett.9b04018. URL: https://doi.org/10.1021/acs.nanolett.9b04018.

[12] Takayuki Ishii et al. “Treatment of cerebral ischemia□reperfusion injury with PEGylated liposomes encapsulating FK506”. en. In: *The FASEB Journal* 27.4 (Apr. 2013), pp. 1362–1370. ISSN: 0892-6638, 1530-6860. DOI: 10.1096/fj.12-221325. URL: https://onlinelibrary.wiley.com/doi/abs/10.1096/fj.12-221325.

[13] Alina Y. Rwei, Weiping Wang, and Daniel S. Kohane. “Photoresponsive nanoparticles for drug delivery”. en. In: *Nano Today* 10.4 (Aug. 2015), pp. 451–467. ISSN: 17480132. DOI: 10.1016/j.nantod.2015.06.004. URL: https://linkinghub.elsevier.com/retrieve/pii/S1748013215000742.

[14] Nicolas Rodriguez, Frédéric Pincet, and Sophie Cribier. “Giant vesicles formed by gentle hydration and electroformation: a comparison by fluorescence microscopy”. eng. In: *Colloids and Surfaces. B, Biointerfaces* 42.2 (May 2005), pp. 125–130. ISSN: 0927-7765. DOI: 10.1016/j.colsurfb.2005.01.010.

[15] Satoshi Hamada et al. “Giant vesicles functionally expressing membrane receptors for an insect pheromone”. en. In: *Chemical Communications* 50.22 (Feb. 2014). Publisher: The Royal Society of Chemistry, pp. 2958–2961. ISSN: 1364-548X. DOI: 10.1039/C3CC48216B. URL: https://pubs.rsc.org/en/content/articlelanding/2014/cc/c3cc48216b.

[16] Nejat Duzgunes and Gregory Gregoriadis. “Introduction: The Origins of Liposomes: Alec Bangham at Babraham”. In: *Methods in Enzymology - METH ENZYMOLOGY* 391 (Dec. 2005), pp. 1–3. ISSN: 9780121827960. DOI: 10.1016/S0076-6879(05)91029-X.

[17] L. van Buren. “Synthetic Cell Aspirations: A Toolbox for Building a Membrane Container from the Bottom Up”. en. In: (2022). DOI: 10.4233/uuid:d0b7e1e5-7836-4914-993d-ff83e446a43f. URL: https://repository.tudelft.nl/islandora/object/uuid%3Ad0b7e1e5-7836-4914-993d-ff83e446a43f (visited on 05/27/2024).

[18] Janani Swaminathan and Carsten Ehrhardt. “Liposomes for Pulmonary Drug Delivery”. en. In: *Controlled Pulmonary Drug Delivery*. Ed. by Hugh D.C. Smyth and Anthony J. Hickey. Advances in Delivery Science and Technology. New York, NY: Springer, 2011, pp. 313–334. ISBN: 978-1-4419-9745-6. DOI: 10.1007/978-1-4419-9745-6_14. URL: https://doi.org/10.1007/978-1-4419-9745-6_14.

[19] Yuchen Fan, Maria Marioli, and Kelly Zhang. “Analytical characterization of liposomes and other lipid nanoparticles for drug delivery”. eng. In: *Journal of Pharmaceutical and Biomedical Analysis* 192 (Jan. 2021), p. 113642. ISSN: 1873-264X. DOI: 10.1016/j.jpba.2020.113642.

[20] A.V. Yadav et al. “Stability aspects of liposome”. In: *Indian. J. Pharm. Educ.* 45 (Oct. 2011), pp. 402–413.

[21] *16:0 PC (DPPC) | 63-89-8 | Avanti*. en-US. URL: https://avantilipids.com/product/850355 (visited on 06/15/2024).

[22] *DSPE-PEG(2000) Amine*. en-US. URL: https://avantilipids.com/product/880128 (visited on 06/15/2024).

[23] *Cholesterol Plant Derived | Avanti Research*. en-US. URL: https://avantilipids.com/product/700100 (visited on 06/15/2024).

[24] *18:1 (Δ9-Cis) PC (DOPC) | 4235-95-4 | Avanti*. URL: https://avantilipids.com/product/850375 (visited on 06/15/2024).

[25] W. Helfrich. “Elastic properties of lipid bilayers: theory and possible experiments”. eng. In: *Zeitschrift Fur Naturforschung. Teil C: Biochemie, Biophysik, Biologie, Virologie* 28.11 (1973), pp. 693–703. ISSN: 0341-0471. DOI: 10.1515/znc-1973-11-1209.

[26] *W. Rawicz, K. C.Olbrich, T.McIntosh,D.Needham, and E. A. Evans, Effect of Chain Length andUnsaturation on Elasticity of Lipid Bilayers, Biophysical Journal 79, 328 (2000). - Google’da Ara*. URL: https://www.google.com/search?q=W.+Rawicz%2C+K.+C.Olbrich%2C+T.McIntosh%2CD.Needham%2C+and+E.+A.+Evans%2C+Effect+of+Chain+Length+andUnsaturation+on+Elasticity+of+Lipid+Bilayers%2C+Biophysical+Journal+79%2C+328+(2000).&rlz=1C1ONGR_enNL1072NL1072&oq=W.+Rawicz%2C+K.+C.Olbrich%2C+T.McIntosh%2CD.Needham%2C+and+E.+A.+Evans%2C+Effect+of+Chain+Length+andUnsaturation+on+Elasticity+of+Lipid+Bilayers%2C+Biophysical+Journal+79%2C+328+(2000).&gs_

lcrp=EgZjaHJvbWUyBggAEEUYOdIBBzkxMmowajSoAgCwAgE&sourceid=chrome&ie=UTF-8 (visited on 06/15/2024).

[27] J. R. Henriksen and J. H. Ipsen. “Measurement of membrane elasticity by micro-pipette aspiration”. eng. In: *The European Physical Journal. E, Soft Matter* 14.2 (June 2004), pp. 149–167. ISSN: 1292-8941. DOI: 10.1140/epje/i2003-10146-y.

[28] Hung V. Ly and Marjorie L. Longo. “The Influence of Short-Chain Alcohols on Interfacial Tension, Mechanical Properties, Area/Molecule, and Permeability of Fluid Lipid Bilayers”. In: *Biophysical Journal* 87.2 (Aug. 2004), pp. 1013–1033. ISSN: 0006-3495. DOI: 10.1529/biophysj.103.034280. URL: https://www.sciencedirect.com/science/article/pii/S0006349504735845 (visited on 06/15/2024).

[29] K Olbrich et al. “Water permeability and mechanical strength of polyunsaturated lipid bilayers.” In: *Biophysical Journal* 79.1 (July 2000), pp. 321–327. ISSN: 0006-3495. URL: https://www.ncbi.nlm.nih.gov/pmc/articles/PMC1300936/ (visited on 06/15/2024).

[30] Andrej Shevchenko and Kai Simons. “Lipidomics: coming to grips with lipid diversity”. en. In: *Nature Reviews Molecular Cell Biology* 11.8 (Aug. 2010). Publisher: Nature Publishing Group, pp. 593–598. ISSN: 1471-0080. DOI: 10.1038/nrm2934. URL: https://www.nature.com/articles/nrm2934 (visited on 06/15/2024).

[31] *Understanding the diversity of membrane lipid composition | Nature Reviews Molecular Cell Biology*. URL: https://www.nature.com/articles/nrm.2017.138 (visited on 06/15/2024).

[32] Abolfazl Akbarzadeh et al. “Liposome: classification, preparation, and applications”. eng. In: *Nanoscale Research Letters* 8.1 (Feb. 2013), p. 102. ISSN: 1931-7573. DOI: 10.1186/1556-276X-8-102.

[33] Andreas Weinberger et al. “Gel-Assisted Formation of Giant Unilamellar Vesicles”. en. In: *Biophysical Journal* 105.1 (July 2013). Publisher: The Biophysical Society, p. 154. DOI: 10.1016/j.bpj.2013.05.024. URL: https://www.ncbi.nlm.nih.gov/pmc/articles/PMC3699747/.

[34] Karthika S. Nair and Harsha Bajaj. “Advances in giant unilamellar vesicle preparation techniques and applications”. In: *Advances in Colloid and Interface Science* 318 (Aug. 2023), p. 102935. ISSN: 0001-8686. DOI: 10.1016/j.cis.2023.102935. URL: https://www.sciencedirect.com/science/article/pii/S0001868623001021 (visited on 06/15/2024).

[35] Mariem Souissi et al. “Integrin-Functionalised Giant Unilamellar Vesicles via Gel-Assisted Formation: Good Practices and Pitfalls”. en. In: *International Journal of Molecular Sciences* 22.12 (Jan. 2021). Number: 12 Publisher: Multidisciplinary Digital Publishing Institute, p. 6335. ISSN: 1422-0067. DOI: 10.3390/ijms22126335. URL: https://www.mdpi.com/1422-0067/22/12/6335 (visited on 06/15/2024).

[36] Lennard van Buren, Gijsje Hendrika Koenderink, and Cristina Martinez-Torres. “DisGUVery: A Versatile Open-Source Software for High-Throughput Image Analysis of Giant Unilamellar Vesicles”. In: *ACS Synthetic Biology* 12.1 (Jan. 2023). Publisher: American Chemical Society, pp. 120–135. DOI: 10.1021/acssynbio.2c00407. URL: https://doi.org/10.1021/acssynbio.2c00407 (visited on 06/12/2024).

[37] Qiong Wang et al. “Formation of Giant Lipid Vesicles in the Presence of Nonelectrolytes—Glucose, Sucrose, Sorbitol and Ethanol”. en. In: *Processes* 9.6 (June 2021). Number: 6 Publisher: Multidisciplinary Digital Publishing Institute, p. 945. ISSN: 2227-9717. DOI: 10.3390/pr9060945. URL: https://www.mdpi.com/2227-9717/9/6/945 (visited on 07/03/2024).

[38] John F. Nagle et al. “What are the true values of the bending modulus of simple lipid bilayers?” eng. In: *Chemistry and Physics of Lipids* 185 (Jan. 2015), pp. 3–10. ISSN: 1873-2941. DOI: 10.1016/j.chemphyslip.2014.04.003.

[39] Michael J. Sanderson et al. “Fluorescence Microscopy”. In: *Cold Spring Harbor protocols* 2014.10 (Oct. 2014), pdb.top071795. ISSN: 1940-3402. DOI: 10.1101/pdb.top071795. URL: https://www.ncbi.nlm.nih.gov/pmc/articles/PMC4711767/ (visited on 06/15/2024).

[40] *Introduction to Fluorescence Microscopy*. URL: https://www.microscopyu.com/techniques/fluorescence/introduction-to-fluorescence-microscopy (visited on 06/15/2024).

[41] *Fluorescence Microscopy: An Easy Guide for Biologists*. en-US. Section: Microscopy and Imaging. Dec. 2022. URL: https://bitesizebio.com/33529/fluorescence-microscopy-the-magic-of-fluorophores-and-filters/ (visited on 06/15/2024).

[42] Zvonimir Boban et al. "Giant Unilamellar Vesicle Electroformation: What to Use, What to Avoid, and How to Quantify the Results". In: *Membranes* 11.11 (Nov. 2021), p. 860. ISSN: 2077-0375. DOI: 10.3390/membranes11110860. URL: https://www.ncbi.nlm.nih.gov/pmc/articles/PMC8622294/ (visited on 06/15/2024).

[43] *ImageJ*. URL: https://imagej.github.io/software/imagej/index (visited on 06/30/2024).

[44] Caroline A. Schneider, Wayne S. Rasband, and Kevin W. Eliceiri. "NIH Image to ImageJ: 25 years of image analysis". en. In: *Nature Methods* 9.7 (July 2012). Publisher: Nature Publishing Group, pp. 671–675. ISSN: 1548-7105. DOI: 10.1038/nmeth.2089. URL: https://www.nature.com/articles/nmeth.2089 (visited on 06/29/2024).

[45] J. C. Stewart. "Colorimetric determination of phospholipids with ammonium ferrothiocyanate". eng. In: *Analytical Biochemistry* 104.1 (May 1980), pp. 10–14. ISSN: 0003-2697. DOI: 10.1016/0003-2697(80)90269-9.

[46] Najla M. Salkho et al. "Photo-Induced Drug Release from Polymeric Micelles and Liposomes: Phototriggering Mechanisms in Drug Delivery Systems". en. In: *Polymers* 14.7 (Mar. 2022), p. 1286. ISSN: 2073-4360. DOI: 10.3390/polym14071286. URL: https://www.mdpi.com/2073-4360/14/7/1286.

[47] Wenjie Chen, Ewa M. Goldys, and Wei Deng. "Light-induced liposomes for cancer therapeutics". en. In: *Progress in Lipid Research* 79 (July 2020), p. 101052. ISSN: 01637827. DOI: 10.1016/j.plipres.2020.101052. URL: https://linkinghub.elsevier.com/retrieve/pii/S0163782720300321.

[48] Brad Kelechava. *ANSI Z136.1-2022: Safe Use of Lasers - ANSI Blog*. en-US. Mar. 2023. URL: https://blog.ansi.org/ansi-z136-1-2022-safe-use-of-lasers/.

[49] Zheng Yuan et al. "Repetitive drug delivery using Light-Activated liposomes for potential antimicrobial therapies". en. In: *Advanced Drug Delivery Reviews* 187 (Aug. 2022), p. 114395. ISSN: 0169409X. DOI: 10.1016/j.addr.2022.114395. URL: https://linkinghub.elsevier.com/retrieve/pii/S0169409X2200285X.

[50] Dyego Miranda and Jonathan F. Lovell. "Mechanisms of light□induced liposome permeabilization". In: *Bioengineering & Translational Medicine* 1.3 (Sept. 2016), pp. 267–276. ISSN: 2380-6761. DOI: 10.1002/btm2.10032. URL: https://www.ncbi.nlm.nih.gov/pmc/articles/PMC5370588/.

[51] Andrew A. Beharry, Oleg Sadovski, and G. Andrew Woolley. "Azobenzene photoswitching without ultraviolet light". eng. In: *Journal of the American Chemical Society* 133.49 (Dec. 2011), pp. 19684–19687. ISSN: 1520-5126. DOI: 10.1021/ja209239m.

[52] Amichai Yavlovich et al. "DESIGN OF LIPOSOMES CONTAINING PHOTOPOLYMERIZABLE PHOSPHOLIPIDS FOR TRIGGERED RELEASE OF CONTENTS". eng. In: *Journal of Thermal Analysis and Calorimetry* 98.1 (Oct. 2009), pp. 97–104. ISSN: 1388-6150. DOI: 10.1007/s10973-009-0228-8.

[53] Binita Chandra, Sanku Mallik, and D. K. Srivastava. "Design of photocleavable lipids and their application in liposomal "uncorking"". eng. In: *Chemical Communications (Cambridge, England)* 24 (June 2005), pp. 3021–3023. ISSN: 1359-7345. DOI: 10.1039/b503423j.

[54] Binita Chandra et al. "Formulation of photocleavable liposomes and the mechanism of their content release". eng. In: *Organic & Biomolecular Chemistry* 4.9 (May 2006), pp. 1730–1740. ISSN: 1477-0520. DOI: 10.1039/b518359f.

[55] Andrew M. Bayer et al. "Triggered liposomal release through a synthetic phosphatidylcholine analogue bearing a photocleavable moiety embedded within the sn-2 acyl chain". eng. In: *Chemistry (Weinheim an Der Bergstrasse, Germany)* 20.12 (Mar. 2014), pp. 3350–3357. ISSN: 1521-3765. DOI: 10.1002/chem.201304094.

[56] Benoît D'Autréaux and Michel B. Toledano. "ROS as signalling molecules: mechanisms that generate specificity in ROS homeostasis". eng. In: *Nature Reviews. Molecular Cell Biology* 8.10 (Oct. 2007), pp. 813–824. ISSN: 1471-0080. DOI: 10.1038/nrm2256.

[57] Alina Pashkovskaya et al. "Light-Triggered Liposomal Release: Membrane Permeabilization by Photodynamic Action". en. In: *Langmuir* 26.8 (Apr. 2010), pp. 5726–5733. ISSN: 0743-7463, 1520-5827. DOI: 10.1021/la903867a. URL: https://pubs.acs.org/doi/10.1021/la903867a.

[58] Paula Enzian et al. "Optically Controlled Drug Release from Light-Sensitive Liposomes with the New Photosensitizer 5,10-DiOH". In: *Molecular Pharmaceutics* 17.8 (Aug. 2020). Publisher: American Chemical Society, pp. 2779–2788. ISSN: 1543-8384. DOI: 10.1021/acs.molpharmaceut.9b01173. URL: https://doi.org/10.1021/acs.molpharmaceut.9b01173.

[59] Jian You et al. "Near-infrared light sensitive liposomes for the enhanced photothermal tumor treatment by the combination with chemotherapy". In: *Pharmaceutical research* 31.3 (Mar. 2014), pp. 554–565. ISSN: 0724-8741. DOI: 10.1007/s11095-013-1180-7. URL: https://www.ncbi.nlm.nih.gov/pmc/articles/PMC4126419/.

[60] Yuan Tang and Anthony J. McGoron. "Combined effects of laser-ICG photothermotherapy and doxorubicin chemotherapy on ovarian cancer cells". In: *Journal of Photochemistry and Photobiology B: Biology* 97.3 (Dec. 2009), pp. 138–144. ISSN: 1011-1344. DOI: 10.1016/j.jphotobiol.2009.09.001. URL: https://www.sciencedirect.com/science/article/pii/S1011134409001663.

[61] Jinxing Chen et al. "Plasmonic Nanostructures for Photothermal Conversion". In: *Small Science* 1 (Jan. 2021), p. 2000055. DOI: 10.1002/smsc.202000055.

[62] Joshua Jackman et al. "Quantitative Profiling of Nanoscale Liposome Deformation by a Localized Surface Plasmon Resonance Sensor". In: *Analytical chemistry* 89 (Dec. 2016). DOI: 10.1021/acs.analchem.6b02532.

[63] Sabrina Simoncelli et al. "Nanoscale Control of Molecular Self-Assembly Induced by Plasmonic Hot-Electron Dynamics". In: *ACS Nano* 12.3 (Mar. 2018). Publisher: American Chemical Society, pp. 2184–2192. ISSN: 1936-0851. DOI: 10.1021/acsnano.7b08563. URL: https://doi.org/10.1021/acsnano.7b08563.

[64] Gil Aizik et al. "Liposomes of Quantum Dots Configured for Passive and Active Delivery to Tumor Tissue". In: *Nano Letters* 19.9 (Sept. 2019). Publisher: American Chemical Society, pp. 5844–5852. ISSN: 1530-6984. DOI: 10.1021/acs.nanolett.9b01027. URL: https://doi.org/10.1021/acs.nanolett.9b01027.

[65] Shengyong Geng et al. "Synthesis of lipid–black phosphorus quantum dot bilayer vesicles for near-infrared-controlled drug release". en. In: *Chemical Communications* 54.47 (June 2018). Publisher: The Royal Society of Chemistry, pp. 6060–6063. ISSN: 1364-548X. DOI: 10.1039/C8CC03423K. URL: https://pubs.rsc.org/en/content/articlelanding/2018/cc/c8cc03423k.

[66] C. A. Robertson, D. Hawkins Evans, and H. Abrahamse. "Photodynamic therapy (PDT): A short review on cellular mechanisms and cancer research applications for PDT". In: *Journal of Photochemistry and Photobiology B: Biology* 96.1 (July 2009), pp. 1–8. ISSN: 1011-1344. DOI: 10.1016/j.jphotobiol.2009.04.001. URL: https://www.sciencedirect.com/science/article/pii/S1011134409000608.

[67] Sven H. C. Askes, Azadeh Bahreman, and Sylvestre Bonnet. "Activation of a Photodissociative Ruthenium Complex by Triplet–Triplet Annihilation Upconversion in Liposomes". en. In: *Angewandte Chemie International Edition* 53.4 (2014), pp. 1029–1033. ISSN: 1521-3773. DOI: 10.1002/anie.201309389. URL: https://onlinelibrary.wiley.com/doi/abs/10.1002/anie.201309389.

[68] Jyoti Boken et al. "Plasmonic nanoparticles and their analytical applications: A review". In: *Applied Spectroscopy Reviews* 52.9 (Oct. 2017). Publisher: Taylor & Francis, pp. 774–820. ISSN: 0570-4928. DOI: 10.1080/05704928.2017.1312427. URL: https://doi.org/10.1080/05704928.2017.1312427.

[69] Vincenzo Amendola et al. “Surface plasmon resonance in gold nanoparticles: a review”. en. In: *Journal of Physics: Condensed Matter* 29.20 (Apr. 2017). Publisher: IOP Publishing, p. 203002. ISSN: 0953-8984. DOI: 10.1088/1361-648X/aa60f3. URL: https://dx.doi.org/10.1088/1361-648X/aa60f3.

[70] Abdul Ismail Abdul Rani et al. *CURRENT ADVANCES IN MICRODEVICES AND NANOTECHNOLOGY*. May 2019. ISBN: 9789672306252.

[71] Jana Olson et al. “Optical characterization of single plasmonic nanoparticles”. en. In: *Chemical Society Reviews* 44.1 (Dec. 2014). Publisher: The Royal Society of Chemistry, pp. 40–57. ISSN: 1460-4744. DOI: 10.1039/C4CS00131A. URL: https://pubs.rsc.org/en/content/articlelanding/2015/cs/c4cs00131a.

[72] Huakang Yu et al. “Plasmon-enhanced light–matter interactions and applications”. en. In: *npj Computational Materials* 5.1 (Apr. 2019). Number: 1 Publisher: Nature Publishing Group, pp. 1–14. ISSN: 2057-3960. DOI: 10.1038/s41524-019-0184-1. URL: https://www.nature.com/articles/s41524-019-0184-1.

[73] Pieter Kik and Mark Brongersma. “Surface Plasmon Nanophotonics”. In: *Springer Series in Optical Sciences*. Vol. 131. Journal Abbreviation: Springer Series in Optical Sciences. Sept. 2007, pp. 1–9. ISBN: 978-1-4020-4349-9. DOI: 10.1007/978-1-4020-4333-8_1.

[74] Kathryn M. Mayer and Jason H. Hafner. “Localized surface plasmon resonance sensors”. eng. In: *Chemical Reviews* 111.6 (June 2011), pp. 3828–3857. ISSN: 1520-6890. DOI: 10.1021/cr100313v.

[75] *Gold Nanoparticle Properties | Cytodiagnostics Inc*. URL: https://www.cytodiagnostics.com/pages/gold-nanoparticle-properties.

[76] Shaowei Wang et al. “Three-Photon Luminescence of Gold Nanorods and Its Applications for High Contrast Tissue and Deep *In Vivo* Brain Imaging”. en. In: *Theranostics* 5.3 (Jan. 2015). Publisher: Ivyspring International Publisher, pp. 251–266. ISSN: 1838-7640. DOI: 10.7150/thno.10396. URL: https://www.thno.org/v05p0251.htm.

[77] Sourour Idoudi et al. “The Golden Liposomes: Preparation and Biomedical Applications of Gold-Liposome Nanocomposites”. en. In: *Journal of Nanotheranostics* 4.3 (Sept. 2023). Number: 3 Publisher: Multidisciplinary Digital Publishing Institute, pp. 201–227. ISSN: 2624-845X. DOI: 10.3390/jnt4030010. URL: https://www.mdpi.com/2624-845X/4/3/10.

[78] Peter P. Edwards and John Meurig Thomas. “Gold in a Metallic Divided State—From Faraday to Present-Day Nanoscience”. In: *Angewandte Chemie International Edition* 46.29 (2007), pp. 5480–5486. ISSN: 1521-3773. DOI: 10.1002/anie.200700428. URL: https://onlinelibrary.wiley.com/doi/abs/10.1002/anie.200700428.

[79] Marek Grzelczak et al. “Shape control in gold nanoparticle synthesis”. en. In: *Chemical Society Reviews* 37.9 (Aug. 2008). Publisher: The Royal Society of Chemistry, pp. 1783–1791. ISSN: 1460-4744. DOI: 10.1039/B711490G. URL: https://pubs.rsc.org/en/content/articlelanding/2008/cs/b711490g.

[80] Kento Koga, Tatsuaki Tagami, and Tetsuya Ozeki. “Gold nanoparticle-coated thermosensitive liposomes for the triggered release of doxorubicin, and photothermal therapy using a near-infrared laser”. In: *Colloids and Surfaces A: Physicochemical and Engineering Aspects* 626 (Oct. 2021), p. 127038. ISSN: 0927-7757. DOI: 10.1016/j.colsurfa.2021.127038. URL: https://www.sciencedirect.com/science/article/pii/S0927775721009079.

[81] Rochelle Arvizo, Resham Bhattacharya, and Priyabrata Mukherjee. “Gold nanoparticles: opportunities and challenges in nanomedicine”. In: *Expert Opinion on Drug Delivery* 7.6 (June 2010). Publisher: Taylor & Francis, pp. 753–763. ISSN: 1742-5247. DOI: 10.1517/17425241003777010. URL: https://doi.org/10.1517/17425241003777010.

[82] Yechezkel (Chezy) Barenholz. “Doxil® — The first FDA-approved nano-drug: Lessons learned”. In: *Journal of Controlled Release*. Past, current and future applications of liposomes - Grand Challenges and Opportunities in Nanomedicine 160.2 (June 2012), pp. 117–134. ISSN: 0168-3659. DOI: 10.1016/j.jconrel.2012.03.020. URL: https://www.sciencedirect.com/science/article/pii/S0168365912002301.

[83] Tatu Lajunen et al. “Light induced cytosolic drug delivery from liposomes with gold nanoparticles”. eng. In: *Journal of Controlled Release: Official Journal of the Controlled Release Society* 203 (Apr. 2015), pp. 85–98. ISSN: 1873-4995. DOI: 10.1016/j.jconrel.2015.02.028.

[84] M. Fátima Barroso et al. “Gold nanoparticles covalently assembled onto vesicle structures as possible biosensing platform”. eng. In: *Beilstein Journal of Nanotechnology* 7 (2016), pp. 655–663. ISSN: 2190-4286. DOI: 10.3762/bjnano.7.58.

[85] Dan Zhu et al. “Investigating the Intracellular Behaviors of Liposomal Nanohybrids *via* SERS: Insights into the Influence of Metal Nanoparticles”. en. In: *Theranostics* 8.4 (Jan. 2018). Publisher: Ivyspring International Publisher, pp. 941–954. ISSN: 1838-7640. DOI: 10.7150/thno.21173. URL: https://www.thno.org/v08p0941.htm (visited on 06/29/2024).

[86] *Preparation of liposomes encapsulated Epirubicin-gold nanoparticles for Tumor specific delivery and release - IOPscience*. URL: https://iopscience.iop.org/article/10.1088/2057-1976/aac9ec (visited on 06/29/2024).

[87] Gabriela Fabiola □tiufiuc et al. “Synergistical Use of Electrostatic and Hydrophobic Interactions for the Synthesis of a New Class of Multifunctional Nanohybrids: Plasmonic Magneto-Liposomes”. en. In: *Nanomaterials* 9.11 (Nov. 2019). Number: 11 Publisher: Multidisciplinary Digital Publishing Institute, p. 1623. ISSN: 2079-4991. DOI: 10.3390/nano9111623. URL: https://www.mdpi.com/2079-4991/9/11/1623 (visited on 06/29/2024).

[88] Ali Akbar Karimi Zarchi et al. “Synthesis and characterisation of liposomal doxorubicin with loaded gold nanoparticles”. en. In: *IET Nanobiotechnology* 12.6 (2018), pp. 846–849. ISSN: 1751-875X. DOI: 10.1049/iet-nbt.2017.0321. URL: https://onlinelibrary.wiley.com/doi/abs/10.1049/iet-nbt.2017.0321 (visited on 06/29/2024).

[89] Kexin Hou et al. “Green synthesis of gold nanoparticles coated doxorubicin liposomes using procyanidins for light–controlled drug release”. In: *Advanced Powder Technology* 31.8 (Aug. 2020), pp. 3640–3649. ISSN: 0921-8831. DOI: 10.1016/j.apt.2020.07.012. URL: https://www.sciencedirect.com/science/article/pii/S0921883120303484 (visited on 06/29/2024).

[90] Syed Baseeruddin Alvi et al. “Iontophoresis mediated localized delivery of liposomal gold nanoparticles for photothermal and photodynamic therapy of acne”. en. In: *Biomaterials Science* 9.4 (Feb. 2021). Publisher: The Royal Society of Chemistry, pp. 1421–1430. ISSN: 2047-4849. DOI: 10.1039/D0BM01712D. URL: https://pubs.rsc.org/en/content/articlelanding/2021/bm/d0bm01712d (visited on 06/29/2024).

[91] Tapan K. Sau et al. “Controlling loading and optical properties of gold nanoparticles on liposome membranes”. In: *Colloids and Surfaces A: Physicochemical and Engineering Aspects* 342.1 (June 2009), pp. 92–96. ISSN: 0927-7757. DOI: 10.1016/j.colsurfa.2009.04.014. URL: https://www.sciencedirect.com/science/article/pii/S0927775709002210 (visited on 05/27/2024).

[92] Christopher K. Haluska et al. “Photo-activated phase separation in giant vesicles made from different lipid mixtures”. In: *Biochimica et Biophysica Acta (BBA) - Biomembranes* 1818.3 (Mar. 2012), pp. 666–672. ISSN: 0005-2736. DOI: 10.1016/j.bbamem.2011.11.025. URL: https://www.sciencedirect.com/science/article/pii/S0005273611004159 (visited on 06/11/2024).

[93] W. W. Sułkowski et al. “The influence of temperature, cholesterol content and pH on liposome stability”. In: *Journal of Molecular Structure*. MOLECULAR SPECTROSCOPY AND MOLECULAR STRUCTURE 2004 744-747 (June 2005), pp. 737–747. ISSN: 0022-2860. DOI: 10.1016/j.molstruc.2004.11.075. URL: https://www.sciencedirect.com/science/article/pii/S0022286004009779 (visited on 07/01/2024).

[94] Peter Grabitz, Vesselka P. Ivanova, and Thomas Heimburg. “Relaxation Kinetics of Lipid Membranes and Its Relation to the Heat Capacity”. In: *Biophysical Journal* 82.1 (Jan. 2002), pp. 299–309. ISSN: 0006-3495. DOI: 10.1016/S0006-3495(02)75395-2. URL: https://www.sciencedirect.com/science/article/pii/S0006349502753952 (visited on 07/01/2024).

A

Image processing by ImageJ

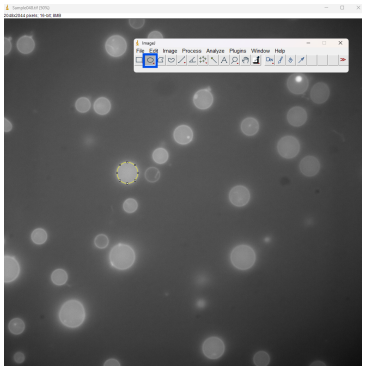

(a) Vesicle detection

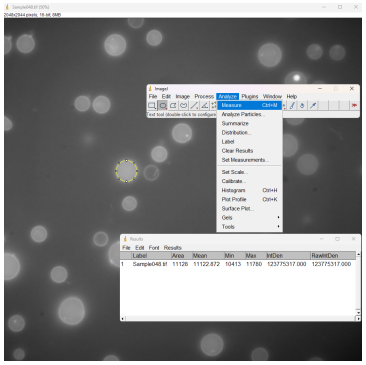

(b) Measuring vesicle properties

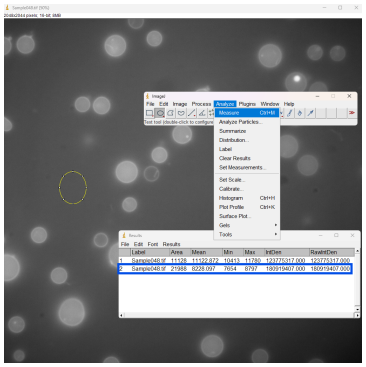

(c) Background detection and measuring

Figure A.1: Image processing by ImageJ

B

Calibration curve for fluorescent intensity

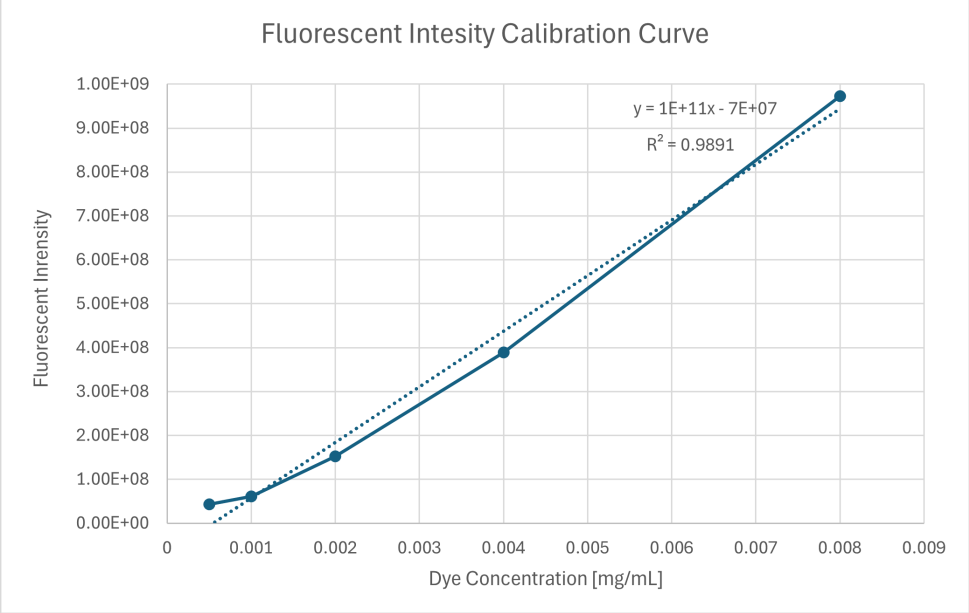

Figure B.1: Fluorescent calibration curve of SRhoB for encapsulation efficiency study (555 nm, 5% intensity, z=3210)

C

Calibration curve for lipid content

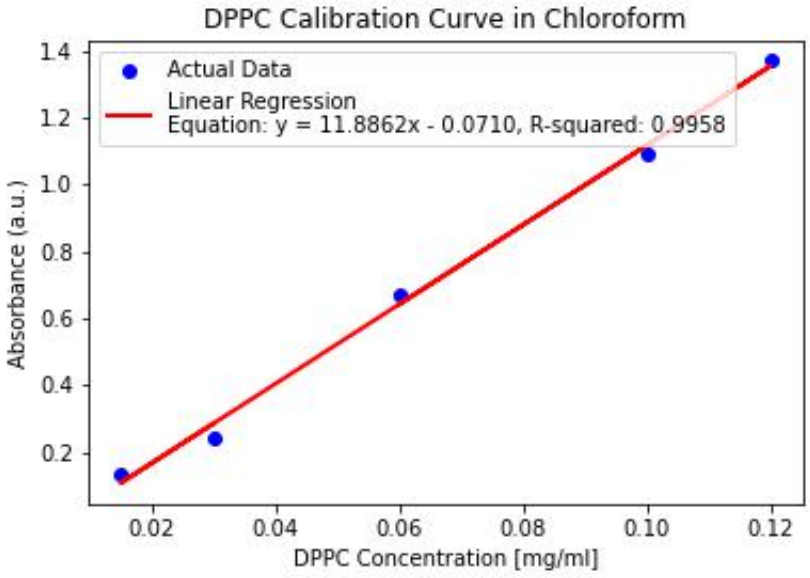

Figure C.1: DPPC calibration curve

D

Stewart assay study

Table 4.1 shows the DPPC-GUV sample volumes used, the dilution factor with chloroform, and the obtained phospholipid content. The results indicated that the Stewart assay is unsuitable for determining the phospholipid content of GUVs. The lipid content varied significantly among GUV volumes, despite measuring the same sample. Adding more DPPC-GUV brought the phospholipid content closer to the theoretical value, but the phase separation became less visible as GUV volume increased. This discrepancy could be due to differences between the thin-film hydration and gel-swelling methods in terms of GUV yield. Since the gel-swelling method uses a very low phospholipid concentration, the number of GUVs obtained is much lower than with the thin-film hydration method, making UV/Vis absorbance measurements unreliable for such low GUV amounts.

Table D.1: Amount of DPPC-GUV samples used for Stewart assay and the resultant phospholipid contents

GUV Volume (µL)	Dilution (µL/µL)	Phospholipid Content (mg/mL)
10	201	1.285
20	101	0.663
50	41	0.286
100	21	0.166
200	11	0.108